Journal of Computational Physics 517 (2024) 113344

Contents lists available at ScienceDirect

Journal of Computational Physics

journal homepage: www.elsevier.com/locate/jcp

A stochastic Galerkin lattice Boltzmann method for incompressible fluid flows with uncertainties

Mingliang Zhong [a,f,*], Tianbai Xiao [b,c], Mathias J. Krause [d,e,f], Martin Frank [a,d], Stephan Simonis [d,f]

[a] Scientific Computing Center, Karlsruhe Institute of Technology, Eggenstein-Leopoldshafen, 76344, Germany
[b] State Key Laboratory of High Temperature Gas Dynamics and Centre for Interdisciplinary Research in Fluids, Institute of Mechanics, Chinese Academy of Sciences, Beijing, 100190, China
[c] School of Engineering Science, University of Chinese Academy of Sciences, Beijing, 100049, China
[d] Institute for Applied and Numerical Mathematics, Karlsruhe Institute of Technology, Karlsruhe, 76131, Germany
[e] Institute of Mechanical Process Engineering and Mechanics, Karlsruhe Institute of Technology, Karlsruhe, 76131, Germany
[f] Lattice Boltzmann Research Group, Karlsruhe Institute of Technology, Karlsruhe, 76131, Germany

ARTICLE INFO

MSC:
65C05
76D06

Keywords:
Stochastic Galerkin method
Generalized polynomial chaos
Uncertainty quantification
Lattice Boltzmann method
Incompressible fluid flow
Computational fluid dynamics
OpenLB

ABSTRACT

Efficient modeling and simulation of uncertainties in computational fluid dynamics (CFD) remains a crucial challenge. In this paper, we present the first stochastic Galerkin (SG) lattice Boltzmann method (LBM) built upon the generalized polynomial chaos (gPC). The proposed method offers an efficient and accurate approach that depicts the propagation of uncertainties in stochastic incompressible flows. Formal analysis shows that the SG LBM preserves the correct Chapman–Enskog asymptotics and recovers the corresponding macroscopic fluid equations. Numerical experiments, including the Taylor–Green vortex flow, lid-driven cavity flow, and isentropic vortex convection, are presented to validate the solution algorithm. The results demonstrate that the SG LBM achieves the expected spectral convergence and the computational cost is significantly reduced compared to the sampling-based non-intrusive approaches, e.g., the routinely used Monte Carlo method. We obtain a speedup factor of 5.72 compared to Monte Carlo sampling in a randomized two-dimensional Taylor–Green vortex flow test case. By leveraging the accuracy and flexibility of LBM and the efficiency of gPC-based SG, the proposed SG LBM provides a powerful framework for uncertainty quantification in CFD practice.

1. Introduction

Uncertainty quantification (UQ) focuses among others on characterizing and analyzing uncertainties present in mathematical models and simulations. It plays a crucial role in providing a comprehensive understanding of the reliability and robustness of predictions and decisions based on these models. Uncertainties can be classified into two main categories: aleatory and epistemic uncertainties. Aleatory uncertainties arise from inherent variability and randomness in the system. For instance, unpredictable turbulence patterns in the atmosphere introduce aleatory uncertainty when simulating airflow over an aircraft wing [1]. Epistemic uncertainties, on the other hand, result from a lack of knowledge or understanding about certain parameters or processes. In the modeling of combustion

* Corresponding author.
E-mail address: mingliang.zhong@kit.edu (M. Zhong).

https://doi.org/10.1016/j.jcp.2024.113344
Received 13 February 2024; Received in revised form 12 July 2024; Accepted 5 August 2024

Available online 13 August 2024

within an engine, uncertainties in precise chemical reaction rates introduce epistemic uncertainty [2]. The goal of UQ is to quantify the impact of these uncertainties on the output of the model and to provide measures of confidence or probability associated with the predictions [3,4].

In the field of computational fluid dynamics (CFD), UQ is receiving increasing attention. CFD simulations encompass various sources of uncertainty, including model parameters, initial conditions, geometry, and boundary conditions [5]. Depending on the coupling approach with CFD, UQ methods can be classified as intrusive or non-intrusive. The non-intrusive method offers a straightforward approach to investigating the forward propagation of uncertainty. Monte Carlo simulation (MCS) is a simple to realize non-intrusive method, where the uncertain parameters are assumed to follow a specific probability distribution, and samples are drawn from the corresponding random space. The deterministic model is then executed using these different samples, and uncertainties are estimated through post-processing. In UQ, MCS results are often regarded as a benchmark for comparison [6]. Although MCS is easy to implement in the deterministic model, its convergence rate remains limited. To address this limitation, alternative methods such as quasi Monte Carlo [7] and multi-level Monte Carlo [8] have been proposed. These methods differ in sample selection and the weights used in the post-processing stage.

Generalized polynomial chaos (gPC) is a widely used UQ method that involves projecting the random solution onto a basis of orthogonal polynomials with respect to the probability distribution of the input random variables [9]. When integrating gPC with the CFD method, two approaches can be adopted. The first approach, similar to MCS [10–13], is stochastic collocation (SC)-based gPC, which utilizes quadrature nodes as samples, performs deterministic model evaluations, and employs weights in the post-processing stage [14–16]. While SC-based gPC improves efficiency compared to MCS, it still faces the challenge of the curse of dimensionality, i.e., the computational cost to reach a certain accuracy exponentially increases with respect to the number of uncertain parameters. In contrast, the stochastic Galerkin (SG)-based gPC method is an intrusive UQ technique that modifies the original numerical model to achieve spectral accuracy [17–21]. Compared to SC-based gPC, SG-based gPC provides a more efficient approximation of uncertain solutions as the residual of the governing equations is orthogonal to the linear space spanned by the polynomial chaos, and the spectral convergence can be achieved provided that the solution depends smoothly on the random parameters [9]. Successful applications in various physical and engineering problems have been demonstrated [22,23]. Moreover, advanced method variants have been proposed, such as the hybrid particle-SG scheme that preserves the main physical properties and the positivity of the reconstructed distribution function, which are often lost in intrusive approaches [24].

The lattice Boltzmann method (LBM) is an efficient mesoscopic CFD method widely used for approximating weakly compressible and incompressible Navier–Stokes equations (NSE) [25–28]. Compared to direct NSE solvers, LBM offers several advantages, including its simplicity in modeling particle interactions rather than solving complex NSE, computational efficiency, and the ability to efficiently handle complex fluid flow phenomena and boundary conditions [29–33]. It is particularly well-suited for simulating flows with intricate geometries, such as those around obstacles [34] or through porous media [35]. Moreover, LBM can effectively leverage parallel computing, enabling the saturation of modern heterogeneous high-performance computing (HPC) machines [36,37]. Although new efficient UQ methods have emerged, UQ still imposes high computational cost requirements. Therefore, it is essential to select a highly efficient CFD solver for studying uncertainty in CFD cases. In this regard, we have chosen LBM due to its remarkable efficiency. To realize this potential, we utilize the platform-agnostic LBM open source framework OpenLB [38,39]. Among others, OpenLB has been used for efficient simulations of turbulent fluid flows [29,40], advection–diffusion processes [41–43] up to ternary fluid mixture flows [39,44], coupled radiative transfer [45], volume-averaged fluid flow [46], fluid–structure interaction [47,48], and indoor thermal comfort [49]. Thus, to feasibly obtain the consistent benchmark UQ data, we implement MCS within the OpenLB framework as the deterministic kernel (see also [42,50]).

Efforts have been made in building intrusive and non-intrusive methods on top of LBM to investigate stochastic flow problems [51, 52]. As the LBM is an established CFD solver, and has the advantage of efficiency, it is mostly used in a non-intrusive approach to, for example in combination with MCS. To overcome the high computational cost of MCS, many alternative approaches have been developed so far, for example using stochastic quadrature points with individual weights to improve the convergence rate [53]. Other UQ methods to substitute the MCS have been proposed for example by Jacob et al. [54] using a c-APK method to study the uncertainty in the urban flow simulation. Wang et al. [55] combined SC-based gPC with LBM to investigate stochastic porous media problems. For the intrusive approach, which has been marginally explored in the context of LBM. For example Fu et al. [51] introduce the SG-based gPC to the finite difference LBM to investigate incompressible viscous flows. Zhao et al. [52] have proposed an LBM approach for the stochastic convection-diffusion equation, employing SG-based gPC on the macroscopic target equations. While previous works demonstrate that LBM can serve as an accurate and efficient CFD solver for stochastic CFD problems, research on an intrusive UQ method for the standard lattice Boltzmann equation remains limited.

In this paper, we extend the LBM by directly implementing the SG method. The key idea is to decompose LBM into polynomials and apply an SG projection to transform the iteration of the velocity distribution function into the iteration of the Fourier coefficients associated with each parameter in LBM. However, there are certain challenges in implementing the SG method in LBM. For instance, the equilibrium distribution function may involve different polynomials. Here, we calculate the product of multiple polynomials at the quadrature points and then derive the Fourier coefficients as a first possible approach. Another consideration is related to the collision term in the SG LBM, which can be solved using either a constant or stochastic relaxation time, depending on the specific requirements of the problem. If we consider viscosity as stochastic, the collision term will inherently become stochastic as well. Given that dimensionless numbers are typically constrained in incompressible laminar scenarios, considering viscosity as stochastic is viable when conducting UQ studies. Therefore, in our study, we uniformly treat the collision term as stochastic. The combination of these two highly efficient methods may offer a promising approach for efficient UQ CFD applications. For this purpose, the present work provides a first proof-of-concept via deriving an intrusive SG LBM and comparing it to non-intrusive MC LBM for simulating viscous

incompressible fluid flow with stochastic initial and boundary conditions. For the latter, we use OpenLB as a deterministic kernel to efficiently produce the MCS reference results and numerically approve the spectral convergence of the SG LBM and show its increased efficiency compared to MC LBM.

This paper is organized as follows: Section 2 presents the incompressible NSE with uncertainty. Section 3 provides a brief introduction to the LBM. Section 4 presents the derivation of applying the SG method on LBM. The numerical results of four test cases, namely the Taylor-Green vortex flow with one and four dimension uncertainty, lid-driven cavity flow, and isentropic vortex convection, are presented in Section 5. Finally, conclusions are drawn in Section 6.

2. Incompressible Navier-Stokes equation with uncertainty

The incompressible NSE is represented as follows:

$$\partial_t \boldsymbol{u} + (\boldsymbol{u}\cdot\boldsymbol{\nabla})\boldsymbol{u} - \nu\boldsymbol{\nabla}^2\boldsymbol{u} = -\frac{1}{\rho}\boldsymbol{\nabla}p + \boldsymbol{f}, \tag{1}$$

$$\boldsymbol{\nabla}\cdot\boldsymbol{u} = 0. \tag{2}$$

Here, ρ denotes fluid density, $\boldsymbol{u}$ represents the velocity vector, p stands for pressure, ν is the dynamic viscosity, and $\boldsymbol{f}$ represents an external force. In our study, the external force is ignored.

The incompressible NSE with uncertainty models fluid flow while considering uncertain parameters. This extension introduces stochastic terms into the deterministic incompressible NSE to account for the variability or lack of precise knowledge in certain parameters.

Hence, we employ the LBM as the discretization method to study the incompressible NSE with uncertainty, which is expressed as:

$$\partial_t \boldsymbol{u}(\boldsymbol{Z}) + (\boldsymbol{u}(\boldsymbol{Z})\cdot\boldsymbol{\nabla})\boldsymbol{u}(\boldsymbol{Z}) - \nu(\boldsymbol{Z})\boldsymbol{\nabla}^2\boldsymbol{u}(\boldsymbol{Z}) = -\frac{1}{\rho}\boldsymbol{\nabla}p(\boldsymbol{Z}), \tag{3}$$

$$\boldsymbol{\nabla}\cdot\boldsymbol{u}(\boldsymbol{Z}) = 0, \tag{4}$$

where, the random vector $\boldsymbol{Z} = (Z_1, ..., Z_d) \in \mathbb{R}^{dZ}$ defined on a probability space $(\Omega, \mathcal{F}, \mathbb{P})$ and taking values in $\mathbb{R}^n$, characterizes the uncertainties of the system. In our paper, both one-dimensional and multi-dimensional uncertainty are studied, we consider two different cases: the velocity $\boldsymbol{u}$ or the viscosity ν, each treated as a separate uncertainty, following the uniform distribution. These can be represented by $\boldsymbol{u}(\boldsymbol{Z})$ and $\nu(\boldsymbol{Z})$. Due to the fact that we consider gPC expansions in the methodology derived below, the validity of our derivations might be restricted to specific probability distributions $\mathcal{F}$ which are summarized for example in [9, Table 5.1].

3. Lattice Boltzmann methods

Forming the centerpiece of any deterministic LBM, the lattice Boltzmann equation (LBE) reads

$$f_i\left(\boldsymbol{x} + \boldsymbol{c}_i\Delta t, t + \Delta t\right) - f_i(\boldsymbol{x}, t) = \Omega_i(\boldsymbol{f}(\boldsymbol{x}, t)), \tag{5}$$

where $i = 0, 1, \ldots, q-1$, the population vector $\boldsymbol{f} \in \mathbb{R}^q$ represents the discretized particle distribution function, $\boldsymbol{c}_i \in \mathbb{R}^d$ denotes the particle speed in the ith velocity direction, and $\boldsymbol{\Omega}(\boldsymbol{f}) \in \mathbb{R}^q$ represents the collision term. Here, the latter is simplified using the Bhatnagar–Gross–Krook (BGK) [56] model

$$\Omega_i(\boldsymbol{f}(\boldsymbol{x}, t)) = -\frac{1}{\tau}\left(f_i(\boldsymbol{x}, t) - f_i^{\mathrm{eq}}(\boldsymbol{x}, t)\right). \tag{6}$$

In (6), $\tau > 0.5$ denotes the relaxation time, while f_i^{eq} represents the equilibrium distribution function given by

$$f_i^{\mathrm{eq}} = w_i\rho\left(1 + \frac{\boldsymbol{u}\cdot\boldsymbol{c}_i}{c_s^2} + \frac{(\boldsymbol{u}\cdot\boldsymbol{c}_i)^2}{2c_s^4} - \frac{\boldsymbol{u}\cdot\boldsymbol{u}}{2c_s^2}\right), \tag{7}$$

where w_i is the weight of each discrete velocity, $\boldsymbol{u}$ denotes the velocity of the particle at position $\boldsymbol{x}$ and time t, and c_s represents the sound speed. The discrete velocity models used in the LBM are characterized by the spatial dimension d and the number of discrete velocities q. Commonly used discrete velocity sets in the form of $DdQq$ are $D1Q3$, $D2Q9$, $D3Q19$. The present study is based on the $D2Q9$ velocity discrete model, where the nine lattice velocities are expressed as

$$\boldsymbol{c}_i = \begin{cases} (0,0) & \text{if } i = 0, \\ (\pm 1, 0), (0, \pm 1) & \text{if } i = 1, 2, \ldots, 4, \\ (\pm 1, \pm 1) & \text{if } i = 5, 6, \ldots, 8, \end{cases} \tag{8}$$

with corresponding weights

$$w_i = w\begin{cases} \frac{4}{9} & \text{if } i = 0, \\ \frac{1}{9} & \text{if } i = 1, 2, \ldots, 4, \\ \frac{1}{36} & \text{if } i = 5, 6, \ldots, 8, \end{cases} \tag{9}$$

where w is the classical weight function in LBM [27]. Based on the above, the flow field is discretized into a square lattice through the space-time variables $\boldsymbol{x}$ and t. Finally, the density ρ and momentum density $\rho\boldsymbol{u}$ approximating the macroscopic unknowns, can be calculated as moments of f_i via

$$\rho(\boldsymbol{x},t)=\sum_{i=0}^{q-1} f_i(\boldsymbol{x},t), \tag{10}$$

$$\rho\boldsymbol{u}(\boldsymbol{x},t)=\sum_{i=0}^{q-1} \boldsymbol{c}_i f_i(\boldsymbol{x},t). \tag{11}$$

Resulting in a perfectly parallelizable numerical scheme, the lattice Boltzmann equation can be decomposed into two distinct steps, reading

$$\text{collision:}\quad f_i^{\star}(\boldsymbol{x},t)=f_i(\boldsymbol{x},t)-\frac{\Delta t}{\tau}\left(f_i(\boldsymbol{x},t)-f_i^{\mathrm{eq}}(\boldsymbol{x},t)\right), \tag{12}$$

$$\text{streaming:}\quad f_i\left(\boldsymbol{x}+\boldsymbol{c}_i\Delta t,t+\Delta t\right)=f_i^{\star}(\boldsymbol{x},t), \tag{13}$$

respectively, where the upper index $\cdot^{\star}$ denotes post-collision variables. In summary, from a kinetic viewpoint, the LBM discretizes velocity, space, and time of the continuous BGK Boltzmann equation. The space-time advancement is achieved through successive evolution of collision and streaming processes, allowing the simulation of fluid flow phenomena with high computational efficiency and mostly second order consistency in space with respect to the incompressible NSE [27,57].

4. Stochastic Galerkin lattice Boltzmann method

4.1. Generalized polynomial expansion of the lattice Boltzmann equation

The generalized polynomial chaos (gPC) method is a numerical technique widely used for uncertainty quantification in complex systems. The gPC method is based on approximating the system's response by expanding it as a polynomial series using orthogonal polynomials. In this study, we consider the model response g as a function of a random vector $\boldsymbol{Z}$ and construct a surrogate representation of g using a truncated series of orthogonal basis functions Φ_α reading

$$g(\boldsymbol{Z})\approx g^N(\boldsymbol{Z})=\sum_{\alpha=0}^{N}\hat{g}_\alpha\Phi_\alpha(\boldsymbol{Z}). \tag{14}$$

In (14), $\hat{g}_\alpha$ represents the αth coefficient of the polynomial expansion, which can be determined through the quadrature rule

$$\hat{g}_\alpha=\frac{1}{\gamma_\alpha}E\left[g^N(\boldsymbol{Z})\Phi_\alpha(\boldsymbol{Z})\right]=\frac{1}{\gamma_\alpha}\int g^N(\boldsymbol{Z})\Phi_\alpha(\boldsymbol{Z})h(\boldsymbol{Z})\,\mathrm{d}\boldsymbol{Z}, \tag{15}$$

where $\gamma_\alpha=E\left[\Phi_\alpha^2\right]$ are the normalization factors, $h(\boldsymbol{Z})$ is the probability density function, the measure $\mathrm{d}\boldsymbol{Z}$ is given by $\mathrm{d}\boldsymbol{Z}=\mathrm{d}Z_1\cdots\mathrm{d}Z_n$.

For a discrete distribution,

$$\hat{g}_\alpha=\frac{1}{\gamma_\alpha}E\left[g^N(\boldsymbol{Z})\Phi_\alpha(\boldsymbol{Z})\right]\approx\frac{1}{\gamma_\alpha}\sum_{j=0}^{M}a_j g\left(\boldsymbol{Q}_j\right)\Phi_\alpha\left(\boldsymbol{Q}_j\right), \tag{16}$$

where a_j are weights, and M is the total number of quadrature points, i.e. the size of the vector $\boldsymbol{Q}\in\mathbb{R}^M$.

The statistics of the model response g are readily available. In our study, we focus on the mean, denoted as $\bar{g}$, and the variance, denoted as $\sigma^2(g)$. $\sigma(g)$ is the standard deviation of the g. These statistics can be calculated as follows:

$$\bar{g}=\int\hat{g}_\alpha\Phi_\alpha(\boldsymbol{Z})\,\mathrm{d}\boldsymbol{Z}=\hat{g}_0 \tag{17}$$

$$\sigma^2(g)=E\left[(g(\boldsymbol{Z})-\bar{g})^2\right]\approx\sum_{\alpha=1}^{N}\hat{g}_\alpha^2 \tag{18}$$

Considering the LBE as a stochastic model, we form the stochastic evolution equation

$$f_i\left(\boldsymbol{x}+\boldsymbol{c}_i\Delta t,t+\Delta t,\boldsymbol{Z}\right)-f_i(\boldsymbol{x},t,\boldsymbol{Z})=\Omega_i\left(\boldsymbol{f}(\boldsymbol{x},t,\boldsymbol{Z})\right), \tag{19}$$

where Z denotes the random input to the model. For all i, we form the gPC expansion of the particle distribution f_i with degree N, so that

$$f_i(\boldsymbol{x},t,\boldsymbol{Z})\approx f_i^N(\boldsymbol{x},t,\boldsymbol{Z})=\sum_{\alpha=0}^{N}\hat{f}_{i\alpha}(\boldsymbol{x},t)\Phi_\alpha(\boldsymbol{Z}). \tag{20}$$

Notably, a gPC approximation of the distribution function f_i could lead to the loss of the positivity of the reconstructed f_i^N, which might cause instability in the gPC system. In some specific configurations of the numerical tests presented in Section 5, non-positivity of populations indeed occurs. From another perspective, hyperbolicity is based on non-negative physical quantities. The LBM does not inherently preserve the hyperbolic nature of the underlying equations, so the non-negativity problem in our proposed system is negligible. To still enforce the positivity of physical quantities, existing filtering strategies could be used [20,24,58].

The stochastic LBM can be expressed in terms of the nonprojected gPC expansion via

$$\text{collision:} \quad f_i^{N,\star}(\boldsymbol{x},t,\boldsymbol{Z}) = f_i^N(\boldsymbol{x},t,\boldsymbol{Z}) - \Omega_i^N\left(\boldsymbol{f}^N(\boldsymbol{x},t,\boldsymbol{Z})\right), \tag{21}$$

$$\text{streaming:} \quad f_i^N\left(\boldsymbol{x}+\boldsymbol{c}_i\Delta t, t+\Delta t, \boldsymbol{Z}\right) = f_i^{N,\star}(\boldsymbol{x},t,\boldsymbol{Z}). \tag{22}$$

By performing the standard SG projection on (21) and (22), we obtain

$$\text{collision:} \quad \widehat{f}_{i\alpha}^{\star}(\boldsymbol{x},t) = \widehat{f}_{i\alpha}(\boldsymbol{x},t) + \widehat{\Omega}_{i\alpha}\left(\boldsymbol{f}^N(\boldsymbol{x},t,\boldsymbol{Z})\right), \tag{23}$$

$$\text{streaming:} \quad \widehat{f}_{i\alpha}\left(\boldsymbol{x}+\boldsymbol{c}_i\Delta t, t+\Delta t\right) = \widehat{f}_{i\alpha}^{\star}(\boldsymbol{x},t), \tag{24}$$

respectively. Note that in the collision step (23), the expansion coefficients $\widehat{f}_{i\alpha}^n$ are updated by adding the contribution from the collision term $\widehat{\boldsymbol{\Omega}}_\alpha(\boldsymbol{f}^{n,N})$. The streaming step (24) only propagates the post-collision expansion coefficients $\widehat{\boldsymbol{f}}_\alpha^{n,\star}$. In summary, equations (23) and (24) describe the Galerkin projection of the LBM using the gPC expansion, allowing for the representation and manipulation of the stochastic variables within the simulation.

4.2. Collision term in generalized polynomial chaos

Regarding the collision term (6), the relaxation time τ and thus the corresponding relaxation frequency $\omega = 1/\tau$ is determined by the kinematic viscosity ν via

$$\nu = c_s^2\left(\tau - \frac{1}{2}\right). \tag{25}$$

In the present setting, the following two distinct cases are to be considered:

1. Deterministic relaxation time: If we assume that the collision frequency is constant, using Galerkin projection the coefficient of the collision term can be easily calculated as

$$\widehat{\Omega}_{i\alpha}\left(\widehat{\boldsymbol{f}}_\alpha(\boldsymbol{x},t)\right) = -\omega\left(\widehat{f}_{i\alpha}(\boldsymbol{x},t) - \widehat{f}_{i\alpha}^{\mathrm{eq}}(\boldsymbol{x},t)\right). \tag{26}$$

2. Stochastic relaxation time: If we consider the kinematic viscosity ν as stochastic, the collision frequency is stochastic, too, and thus should be decomposed with the same polynomial basis and order, i.e.

$$\omega^N(\boldsymbol{Z}) = \sum_{\alpha=0}^{N}\widehat{\omega}_\alpha\Phi_\alpha(\boldsymbol{Z}), \tag{27}$$

where $\widehat{\omega}_\alpha$ are the expansion coefficients. In this case, the collision term is expanded in a different form, namely

$$\Omega_i^N\left(\boldsymbol{f}^N(\boldsymbol{x},t,\boldsymbol{Z})\right) = \omega^N(\boldsymbol{Z})\left(f_i^{\mathrm{eq},N}(\boldsymbol{x},t,\boldsymbol{Z}) - f_i^N(\boldsymbol{x},t,\boldsymbol{Z})\right). \tag{28}$$

Using SG projection once again

$$\widehat{\Omega}_{i\alpha}\left(\widehat{\boldsymbol{f}}_\alpha\right) = \frac{1}{\gamma_\alpha}\left(\sum_{j=0}^{N}\sum_{k=0}^{N}\widehat{\omega}_j\widehat{f}_{i\alpha}^{\mathrm{eq}}E\left[\Phi_j\Phi_k\Phi_\alpha\right] - \sum_{j=0}^{N}\sum_{k=0}^{N}\widehat{\omega}_j\widehat{f}_{i\alpha}E\left[\Phi_j\Phi_k\Phi_\alpha\right]\right). \tag{29}$$

In Equation (29), the collision term coefficients $\widehat{\boldsymbol{\Omega}}_\alpha(\widehat{\boldsymbol{f}}_\alpha)$ are calculated based on the expansion coefficients $\widehat{\omega}_j$ and $\widehat{f}_{i\alpha}$, as well as the quadratures of the products of the orthogonal basis functions Φ_j, Φ_k, and Φ_α. This formulation allows for the treatment of stochastic kinematic viscosity and provides a novel way to incorporate the stochastic nature of the collision term in the LBM. Note that the methodology is similar to the one proposed in [20] for the gas kinetic scheme.

4.3. Moments and equilibrium populations in generalized polynomial chaos

In the deterministic LBE (5), obtaining the equilibrium distribution function is straight-forward using (7). However, in the stochastic system, direct multiplication and division cannot be applied to the stochastic moments. Therefore, we propose a method to obtain stochastic moments based on the existing stochastic distribution function and lattice velocity. The moments are defined as

$$\rho^N(\boldsymbol{Z}) = \sum_{i=0}^{8}\sum_{\alpha=0}^{N}\widehat{f}_{i\alpha}\Phi_\alpha(\boldsymbol{Z}), \tag{30}$$

$$(\rho \boldsymbol{u})^N(\boldsymbol{Z}) = \sum_{i=0}^{8} \sum_{\alpha=0}^{N} \widehat{f}_{i\alpha} \boldsymbol{c}_i \Phi_\alpha(\boldsymbol{Z}). \tag{31}$$

By calculating the moments on quadrature points Q_j, for $j = 0, 1, \ldots, M$ we can directly obtain the velocity on those quadrature points via

$$\boldsymbol{u}^N(Q_j) = \frac{(\rho \boldsymbol{u})^N(Q_j)}{\rho^N(Q_j)}. \tag{32}$$

To calculate the equilibrium populations on the quadrature points Q_j, we use the velocity and density on the same quadrature points, so that

$$f_i^{\mathrm{eq},N}(\boldsymbol{x}, t, Q_j) = w_i \rho^N(Q_j) \left(1 + \frac{\boldsymbol{u}^N(Q_j) \cdot \boldsymbol{c}_i}{c_s^2} + \frac{\left(\boldsymbol{u}^N(Q_j) \cdot \boldsymbol{c}_i\right)^2}{2c_s^4} - \frac{\boldsymbol{u}^N(Q_j) \cdot \boldsymbol{u}^N(Q_j)}{2c_s^2}\right). \tag{33}$$

Next, we decompose the equilibrium distribution into a gPC expansion

$$f_i^{\mathrm{eq},N}(\boldsymbol{x}, t, \boldsymbol{Z}) = \sum_{\alpha=0}^{N} \widehat{f}_{i\alpha}^{\mathrm{eq}} \Phi_\alpha(\boldsymbol{Z}) \tag{34}$$

The coefficients of the equilibrium distribution function are calculated using a quadrature rule

$$\widehat{f}_{i\alpha}^{\mathrm{eq}} = \frac{E\left[f_i^{\mathrm{eq},N}(\boldsymbol{x}, t, \boldsymbol{Z}) \Phi_\alpha(\boldsymbol{Z})\right]}{E\left[\Phi_\alpha^2(\boldsymbol{Z})\right]}, \tag{35}$$

for all $i = 0, 1, \ldots q-1$. When combined, the above expressions (30), (31), (32), (33), (34), and (35) provide a clear description of the moments and the computation of the equilibrium distribution function within the gPC expansion.

4.4. Chapman–Enskog expansion analysis

We use the Chapman–Enskog (CE) expansion to provide a formal consistency analysis of the proposed SG LBM in terms of orders of magnitude $\mathcal{O}(\cdot)$ obtained in a multi-scale expansion. To the knowledge of the authors, this is the first CE expansion analysis of an SG LBM. For simplicity, we assume deterministic relaxation according to (25) and nondimensionalize the relaxation time. Since LBE asymptotically approaches the incompressible NSE, we directly make the incompressibility assumption.

With that, we start with the gPC expanded SG LBE

$$\widehat{f}_{i\alpha}\left(\boldsymbol{x} + \boldsymbol{c}_i \Delta t, t + \Delta t\right) = \widehat{f}_{i\alpha}(\boldsymbol{x}, t) - \Delta t \omega \left(\widehat{f}_{i\alpha}(\boldsymbol{x}, t) - \widehat{f}_{i\alpha}^{\mathrm{eq}}(\boldsymbol{x}, t)\right). \tag{36}$$

The expansion coefficients of the density distribution function, the temporal and the spatial derivatives are expanded as

$$\widehat{f}_{i\alpha} = \sum_{k=0}^{\infty} \varepsilon^k \widehat{f}_{i\alpha}^{(k)}, \tag{37}$$

$$\partial_t = \varepsilon \partial_t^{(1)} + \varepsilon^2 \partial_t^{(2)}, \tag{38}$$

$$\boldsymbol{\nabla} = \varepsilon \boldsymbol{\nabla}^{(1)}, \tag{39}$$

respectively, where $\partial_\cdot = \partial/(\partial \cdot)$ denotes the partial derivative with respect to $\cdot$, and $\varepsilon > 0$ is an expansion parameter which indicates the terms of order $\mathcal{O}(Kn)$ with the Knudsen number denoted as Kn. Using a Taylor expansion, the SG LBE (36) becomes

$$\Delta t \left(\partial_t + \boldsymbol{c}_i \cdot \boldsymbol{\nabla}\right) \widehat{f}_{i\alpha} + \frac{\Delta t^2}{2} \left(\partial_t + \boldsymbol{c}_i \cdot \boldsymbol{\nabla}\right)^2 \widehat{f}_{i\alpha} + \Delta t \omega \left(\widehat{f}_{i\alpha} - \widehat{f}_{i\alpha}^{\mathrm{eq}}\right) = \mathcal{O}\left(\Delta t^3\right). \tag{40}$$

Neglecting terms of $\mathcal{O}(\Delta t^3)$ and higher, and substituting the multi-scale expansions (37), (38), and (39) into (40), we can split the equation in terms of orders of magnitudes $\mathcal{O}(\varepsilon^k)$. For $k = 0, 1, 2$, we obtain

$$\mathcal{O}\left(\varepsilon^0\right): \quad \widehat{f}_{i\alpha}^{(0)} - \widehat{f}_{i\alpha}^{\mathrm{eq}} = 0, \tag{41}$$

$$\mathcal{O}\left(\varepsilon^1\right): \quad \left(\partial_t^{(1)} + \boldsymbol{c}_i \cdot \boldsymbol{\nabla}^{(1)}\right) \widehat{f}_{i\alpha}^{(0)} = -\omega \widehat{f}_{i\alpha}^{(1)}, \tag{42}$$

$$\mathcal{O}\left(\varepsilon^2\right): \quad \partial_t^{(2)} \widehat{f}_{i\alpha}^{(0)} + \left(1 - \frac{1}{2}\Delta t \omega\right) \left(\partial_t^{(1)} + \boldsymbol{c}_i \cdot \boldsymbol{\nabla}^{(1)}\right) \widehat{f}_{i\alpha}^{(1)} = -\omega \widehat{f}_{i\alpha}^{(2)}, \tag{43}$$

respectively. Obviously, from (41), we have that $\widehat{f}_{i\alpha}^{(0)} = \widehat{f}_{i\alpha}^{\mathrm{eq}}$. To proceed with the CE analysis, we form a gPC expansion of the stochastic density and the stochastic momentum density via

$$\rho^N(\boldsymbol{x}, t, \boldsymbol{Z}) = \sum_{\alpha=0}^{N} \widehat{\rho}_\alpha(\boldsymbol{x}, t) \Phi_\alpha(\boldsymbol{Z}), \tag{44}$$

$$(\rho \boldsymbol{u})^N(\boldsymbol{x},t,\boldsymbol{Z}) = \sum_{\alpha=0}^{N} \left(\widehat{\rho \boldsymbol{u}}\right)_\alpha (\boldsymbol{x},t)\,\Phi_\alpha(\boldsymbol{Z}), \tag{45}$$

respectively, where

$$\widehat{\rho}_\alpha(\boldsymbol{x},t) = \sum_{i=0}^{q-1} \widehat{f}_{i\alpha}(\boldsymbol{x},t), \tag{46}$$

$$\left(\widehat{\rho \boldsymbol{u}}\right)_\alpha(\boldsymbol{x},t) = \sum_{i=0}^{q-1} \boldsymbol{c}_i \widehat{f}_{i\alpha}(\boldsymbol{x},t). \tag{47}$$

To restore the stochastic macroscopic equation, the equilibrium distribution should meet the requirements of the following equations:

$$\sum_i \widehat{f}^{eq}_{i\alpha} = \widehat{\rho}_\alpha, \tag{48}$$

$$\sum_i \boldsymbol{c}_i \widehat{f}^{eq}_{i\alpha} = \widehat{\rho \boldsymbol{u}}_\alpha. \tag{49}$$

Here, we make an assumption that the density is asymptotically constant in incompressible fluids, which yields

$$\widehat{\boldsymbol{u}}_\alpha = \frac{\left(\widehat{\rho \boldsymbol{u}}\right)_\alpha}{\widehat{\rho}_\alpha}. \tag{50}$$

Simultaneously, with equations (46), (47), (48), and (49), we can easily obtain

$$\sum_n f^{(n)}_{i\alpha} = 0, \quad \forall n \neq 0, \tag{51}$$

$$\sum_n \boldsymbol{c}_i f^{(n)}_{i\alpha} = 0, \quad \forall n \neq 0. \tag{52}$$

Thus, the zeroth and first order moment summation (42) are

$$\partial_t^{(1)} \widehat{\rho} + \boldsymbol{\nabla}^{(1)} \cdot (\widehat{\rho \boldsymbol{u}}) = 0, \tag{53}$$

$$\partial_t^{(1)} \widehat{\rho \boldsymbol{u}}_b + \boldsymbol{\nabla}^{(1)} \cdot \left(\widehat{\rho \boldsymbol{u}_a \boldsymbol{u}_b}\right) = -\boldsymbol{\nabla}^{(1)} \widehat{p}. \tag{54}$$

The zeroth and first order moment summation (43) are

$$\partial_t^{(2)} \widehat{\rho} = 0, \tag{55}$$

$$\partial_t^{(2)} \widehat{\rho \boldsymbol{u}}_b + \left(1 - \frac{\omega}{2}\right) \boldsymbol{\nabla}^{(1)} \cdot \left(\sum_i \boldsymbol{c}_{ia} \boldsymbol{c}_{ib} \widehat{f}^{(1)}_{i\alpha}\right) = 0. \tag{56}$$

Finally, with the help of (42), we obtain

$$\sum_i \boldsymbol{c}_{ia} \boldsymbol{c}_{ib} \widehat{f}^{(1)}_{i\alpha} = -\frac{1}{\omega}\left[\partial_t^{(1)}\left((\widehat{\rho \boldsymbol{u}_a \boldsymbol{u}_b})_\alpha + \widehat{\rho}_\alpha c_s^2 \delta_{ab}\right) + \boldsymbol{\nabla}^{(1)} \cdot \left(\sum_i \boldsymbol{c}_{ia} \boldsymbol{c}_{ib} \boldsymbol{c}_{ic} \widehat{f}^{eq}_{i\alpha}\right)\right] \tag{57}$$

$$\partial_t^{(1)}\left((\widehat{\rho \boldsymbol{u}_a \boldsymbol{u}_b})_\alpha + \widehat{\rho}_\alpha c_s^2 \delta_{ab}\right) = \partial_t^{(1)}\left(\widehat{\rho \boldsymbol{u}_a \boldsymbol{u}_b}\right)_\alpha + c_s^2 \boldsymbol{\nabla}^{(1)} \cdot (\widehat{\rho \boldsymbol{u}}_\alpha) \delta_{ab}. \tag{58}$$

Note that the deterministic term $\partial_t^{(1)}\left(\rho \boldsymbol{u}_a \boldsymbol{u}_b\right)$ can be expanded as

$$\partial_t^{(1)}\left(\rho \boldsymbol{u}_a \boldsymbol{u}_b\right) = -c_s^2 \boldsymbol{u}_a \boldsymbol{\nabla} \cdot \rho - c_s^2 \boldsymbol{u}_b \nabla \cdot \rho - \boldsymbol{\nabla} \cdot (\rho \boldsymbol{u}_a \boldsymbol{u}_b \boldsymbol{u}_c). \tag{59}$$

In (59), under the incompressibility assumption, the density is asymptotically constant, allowing for the cancellation of the first two terms on the right. Moreover, the velocity in incompressible flow is significantly lower than the sound speed. By using the sound speed to make the last term dimensionless, it becomes a third-order small quantity, which can also be neglected. This implies that the term $\partial_t^{(1)}\left(\rho \boldsymbol{u}_a \boldsymbol{u}_b\right)$ can be disregarded under the incompressibility assumption. Therefore, its gPC coefficient, $\partial t^{(1)}(\widehat{\rho \boldsymbol{u}_a \boldsymbol{u}_b})_\alpha$, can be assumed to be negligible. Considering the latticed equilibrium distribution function, with a simple algebra we have that

$$\boldsymbol{\nabla}^{(1)} \cdot \left(\sum_i \boldsymbol{c}_{ia} \boldsymbol{c}_{ib} \boldsymbol{c}_{ic} \widehat{f}^{eq}_{i\alpha}\right) = c_s^2 \boldsymbol{\nabla}^{(1)} \cdot (\widehat{\rho \boldsymbol{u}}) \delta_{ab} + \widehat{\rho} c_s^2 (\boldsymbol{\nabla} \cdot \widehat{\boldsymbol{u}}_a + \boldsymbol{\nabla} \cdot \widehat{\boldsymbol{u}}_b). \tag{60}$$

After sorting terms, we observe that

$$\partial_t \widehat{\rho}_\alpha + \boldsymbol{\nabla} \cdot \left(\widehat{\rho \boldsymbol{u}}\right)_\alpha = 0, \tag{61}$$

$$\partial_t \left(\widehat{\rho \boldsymbol{u}}\right)_\alpha + \boldsymbol{\nabla} \cdot \left(\left(\widehat{\rho \boldsymbol{u}}\right)_\alpha \otimes \widehat{\boldsymbol{u}}_\alpha\right) = -\boldsymbol{\nabla} \widehat{p}_\alpha + \mu \boldsymbol{\nabla} \cdot \left[\boldsymbol{\nabla} \widehat{\boldsymbol{u}}_\alpha + \left(\boldsymbol{\nabla} \widehat{\boldsymbol{u}}_\alpha\right)^{\mathrm{T}}\right], \tag{62}$$

where the pressure expansion coefficient is defined as $\widehat{p}_\alpha = c_s^2 \widehat{\rho}_\alpha$. Again, assuming asymptotically incompressible flow, (61) becomes

$$\boldsymbol{\nabla} \cdot \widehat{\boldsymbol{u}}_\alpha = 0. \tag{63}$$

Then, using the classical simplification steps for modeling deterministic incompressible fluid flow based on the weakly compressible NSE, e.g. $\boldsymbol{\nabla} \cdot \left(\boldsymbol{\nabla} \widehat{\boldsymbol{u}}_\alpha\right)^{\mathrm{T}} = \boldsymbol{\nabla} \left(\boldsymbol{\nabla} \cdot \widehat{\boldsymbol{u}}_\alpha\right) = 0$, can be used in (61) and (62). Based on that, it is observed that (61) and (62) structurally correspond to the stochastic weakly compressible NSE in terms of expansion coefficient variables $\widehat{\rho}_\alpha$ and $\left(\widehat{\rho \boldsymbol{u}}\right)_\alpha$. Conclusively, we thus have formally proven the consistency of order two of the proposed SG LBM to stochastic density and density momentum moments (30) and (31), respectively.

4.5. Lattice Boltzmann boundary conditions in generalized polynomial chaos

4.5.1. No-slip wall boundary condition

The classical implementation of the mesoscopic bounce-back boundary condition for obtaining a macroscopic no-slip wall for the fluid velocity used in the present configuration. The standard streaming is replaced by switching the distribution function in the opposite velocity direction (see e.g. [59] and references therein). For our SG LBM, the expansion coefficients are switched instead of the distribution function. For example, in a specific setting in two dimensions, the coefficient for the incoming distribution function $\widehat{f}_{2\alpha}^{\mathrm{eq}}$ is set equal to the coefficient of the outgoing distribution function $\widehat{f}_{4\alpha}^{\mathrm{eq}}$.

$$\widehat{f}_{2\alpha}\left(\mathbf{x}_b, t + \Delta t\right) = \widehat{f}_{4\alpha}^{\star}\left(\mathbf{x}_b, t\right), \tag{64}$$

$$\widehat{f}_{5\alpha}\left(\mathbf{x}_b, t + \Delta t\right) = \widehat{f}_{7\alpha}^{\star}\left(\mathbf{x}_b, t\right), \tag{65}$$

$$\widehat{f}_{6\alpha}\left(\mathbf{x}_b, t + \Delta t\right) = \widehat{f}_{8\alpha}^{\star}\left(\mathbf{x}_b, t\right). \tag{66}$$

4.5.2. Moving wall boundary condition

For realizing macroscopic moving wall boundary conditions, we adopt the non-equilibrium extrapolation method. In the deterministic non-equilibrium extrapolation method [60], the following steps are performed at time step t_n, wall node $\boldsymbol{x}_{\mathrm{wall}}$, and incoming node $\boldsymbol{x}_{\mathrm{in}}$:

$$\rho\left(\boldsymbol{x}_{\mathrm{wall}}, t_n\right) = \rho\left(\boldsymbol{x}_{\mathrm{in}}, t_n\right), \tag{67}$$

$$\boldsymbol{u}\left(\boldsymbol{x}_{\mathrm{wall}}, t_n\right) = \boldsymbol{u}_{\mathrm{wall}}, \tag{68}$$

$$f_i\left(\boldsymbol{x}_{\mathrm{wall}}, t_n\right) = f_i^{\mathrm{eq}}\left(\boldsymbol{x}_{\mathrm{wall}}, t_n\right) + \left(f_i\left(\boldsymbol{x}_{\mathrm{in}}, t_n\right) - f_i^{\mathrm{eq}}\left(\boldsymbol{x}_{\mathrm{in}}, t_n\right)\right), \tag{69}$$

for all $i = 0, 1, \ldots q-1$, where $\boldsymbol{u}_{\mathrm{wall}}$ denotes the moving wall velocity. To account for the stochastic information, we apply the gPC expansion to (67), (68), and (69), respectively. The resulting stochastic non-equilibrium extrapolation method hence reads

$$\widehat{\rho}_\alpha\left(\boldsymbol{x}_{\mathrm{wall}}, t\right) = \widehat{\rho}_\alpha\left(\boldsymbol{x}_{\mathrm{in}}, t\right), \tag{70}$$

$$\widehat{\boldsymbol{u}}_\alpha\left(\boldsymbol{x}_{\mathrm{wall}}, t\right) = \widehat{\boldsymbol{u}}_{\mathrm{wall}}, \tag{71}$$

$$\widehat{f}_{i\alpha}\left(\boldsymbol{x}_{\mathrm{wall}}, t\right) = \widehat{f}_{i\alpha}^{\mathrm{eq}}\left(\boldsymbol{x}_{\mathrm{wall}}, t\right) + \left(\widehat{f}_{i\alpha}\left(\boldsymbol{x}_{\mathrm{in}}, t\right) - \widehat{f}_{i\alpha}^{\mathrm{eq}}\left(\boldsymbol{x}_{\mathrm{in}}, t\right)\right). \tag{72}$$

4.6. Implementational details

The deterministic LBE updates the distribution function $\boldsymbol{f}$ itself from time step t_n to t_{n+1} (cf. (21) and (22)). However, in the here proposed SG LBM, we update the expansion coefficients $\widehat{\boldsymbol{f}}_\alpha$ of the approximate stochastic distribution function $\boldsymbol{f}^N(\boldsymbol{Z})$ instead. The updating procedure is summarized as follows:

1. Calculate the expansion coefficients $\widehat{f}_{i\alpha}^{\mathrm{eq}}$ using (35).
2. Compute the collision term using either (26) or (29), depending on whether the collision frequency is constant or stochastic.
3. Perform the collision and streaming by applying (23) and (24), respectively. This step involves combining the collision term with the current expansion coefficients to obtain the updated coefficients.
4. Apply the appropriate boundary conditions to ensure the desired behavior at the boundaries of the computational domain.
5. Update the moments of the distribution function using (30), (31) and (32). Based on these equations we calculate the stochastic moments, density $\rho^N(\boldsymbol{Z})$ and velocity $\boldsymbol{u}^N(\boldsymbol{Z})$ using the expansion coefficients $\widehat{f}_{i\alpha}$.

5. Numerical experiments

5.1. Taylor-Green vortex flow

To eliminate the influence of boundary conditions, we select a periodic test case with an analytical solution: the two-dimensional decaying Taylor-Green vortex (TGV) flow. Based on this periodic test case we assess the accuracy and consistency of the here proposed SG LBM. The TGV flow [61], given by

$$\boldsymbol{u}(x,y,t) = \begin{pmatrix} u(x,y,t) \\ v(x,y,t) \end{pmatrix} = \begin{pmatrix} -u_0 \cos\left(k_x x\right) \sin\left(k_y y\right) e^{-\frac{t}{t_d}} \\ u_0 \sin\left(k_x x\right) \cos\left(k_y y\right) e^{\frac{t}{t_d}} \end{pmatrix}, \tag{73}$$

$$p(x,y,t) = -\frac{1}{4}u_0^2 \left[\cos\left(2k_x x\right) + \left(\frac{k_x}{k_y}\right)^2 \cos\left(2k_y y\right)\right] e^{-\frac{2t}{t_d}} + P_0, \tag{74}$$

provides a periodic analytical solution to the two-dimensional incompressible NSE. In (73), the initial velocity amplitude is denoted as $u_0 = 0.01$. Below $\nu > 0$ represents the shear viscosity. The computational domain $\Omega_{\mathbf{\Delta x}} \subseteq \Omega$ is defined with a resolution of $nx \times ny$. In our paper, we choose the same value for nx and ny. The scaling factors $k_x = \frac{2\pi}{nx}$ and $k_y = \frac{2\pi}{ny}$ can be used to scale the size of the flow domain. The characteristic time scale is defined as $t_d = \frac{1}{\nu(k_x^2+k_y^2)}$, and the initial pressure P_0 is set to zero.

The characteristic length, denoted as L, is set to 2π, and the voxel length dx, determined by the resolution, is calculated as L/nx. In our study, we use a Reynolds number of $Re = 15$, and the deterministic viscosity ν_0 is then defined as $\nu_0 = u_0 L/Re$. We have chosen a relaxation time of $\tau = \nu/C_s^2 + 0.5$.

Moreover, by using the LBM-specific relation $\rho = \frac{p}{{c_s}^2}$, where c_s is the speed of sound, we can obtain the initial density condition ρ_0.

In this test case, the normalized total kinetic energy is computed as

$$K(t) = \frac{2}{|\Omega| u_0^2} \int_{\Omega} \left(u^2(x,y,t) + v^2(x,y,t)\right) \mathrm{d}x\mathrm{d}y, \tag{75}$$

where the integral is approximated with averaging over the domain constituted by grid nodes $(x,y) \in [0,nx] \times [0,ny]$. First, we consider the viscosity ν as an uncertain parameter, denoted as $\nu = \xi\nu_0$, where ξ follows a uniform distribution $\xi \sim \mathcal{U}_{[0.8,1.2]}$.

Here, we also apply gPC expansion to the normalized total kinetic energy, which is computed as

$$\widehat{K}_\alpha(t) = \frac{2}{|\Omega| u_0^2} \int_{\Omega} \left((\widehat{u^2})_\alpha(x,y,t) + (\widehat{v^2})_\alpha(x,y,t)\right) \mathrm{d}x\mathrm{d}y, \tag{76}$$

the gPC coefficient for normalized total kinetic energy $\widehat{K}(t)$ is calculated based on the gPC coefficients for the squared velocities $(\widehat{u^2})$ and $(\widehat{v^2})$. These coefficients for the squared velocities are determined as follows:

$$(\widehat{u^2})_\alpha = \sum_{j=0}^{N} \sum_{k=0}^{N} \widehat{u}_j \widehat{u}_\alpha E\left[\phi_j \phi_k \phi_\alpha\right] \tag{77}$$

$$(\widehat{v^2})_\alpha = \sum_{j=0}^{N} \sum_{k=0}^{N} \widehat{v}_j \widehat{v}_\alpha E\left[\phi_j \phi_k \phi_\alpha\right] \tag{78}$$

Across different resolutions, we compare the computed mean of normalized total kinetic energy with its analytical reference at two points in time $t = 0.2t_d$ and $t = 0.5t_d$, respectively.

Initially, we perform a stochastic consistency study for SG LBM on the two-dimensional TGV flow. This evaluation is based on the relative error, denoted as $\delta(t)$, of the mean and standard deviation of normalized total kinetic energy $K(t)$ concerning the results obtained at various points in time, namely, $t = 0.2t_d$ and $0.5t_d$. We investigate this across different spatial resolutions (here $nx = 32, 64, 128, 256$) and polynomial orders ($N = 1, 2, 3, \ldots, 8$). Hence, we compute

$$\delta(t) = \frac{\left|\bar{K}_N^{nx}(t) - \bar{K}_9^{nx}(t)\right|}{\left|\bar{K}_9^{nx}(t)\right|}, \tag{79}$$

$$\delta(t) = \frac{\left|\sigma\left(K_N^{nx}(t)\right) - \sigma\left(K_9^{nx}(t)\right)\right|}{\left|\sigma\left(K_9^{nx}(t)\right)\right|}, \tag{80}$$

respectively. The convergence results in terms of the obtained relative error over several resolutions and polynomial orders are presented in Fig. 1 for two dedicated points in time. The results show that a polynomial order of $N = 5$ is sufficient for achieving the highest accuracy. Hence, all of the following tests use the polynomial order $N = 5$. From Fig. 1, it can be observed that the relative errors converge exponentially to machine precision. This indicates that the here proposed SG LBM achieves spectral accuracy in the random space.

Moreover, we assess the spatial consistency of SG LBM by measuring the experimental order of convergence (EOC). This is done by comparing the results obtained at different resolutions with the analytical solution at the highest resolution. To validate the spatial consistency of our proposed method, we implemented it using a polynomial order of $N = 5$ and compute the following error

$$\delta = \frac{\left|\bar{K}_5^{nx}(t) - K^{128}(t)\right|}{\left|K^{128}(t)\right|}, \tag{81}$$

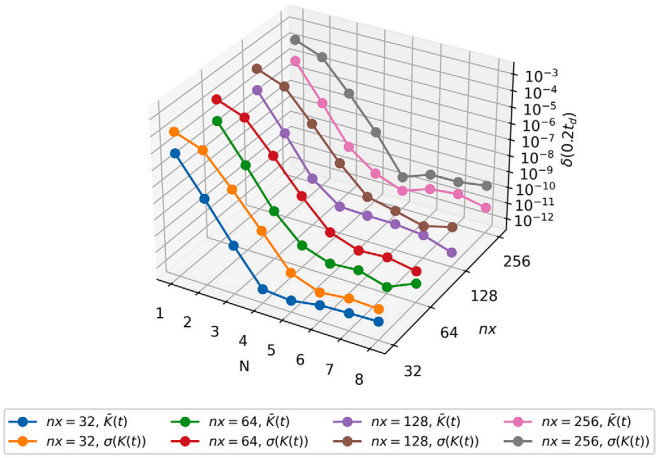

(a) Relative error $(\delta(t))$ at $t = 0.2t_d$

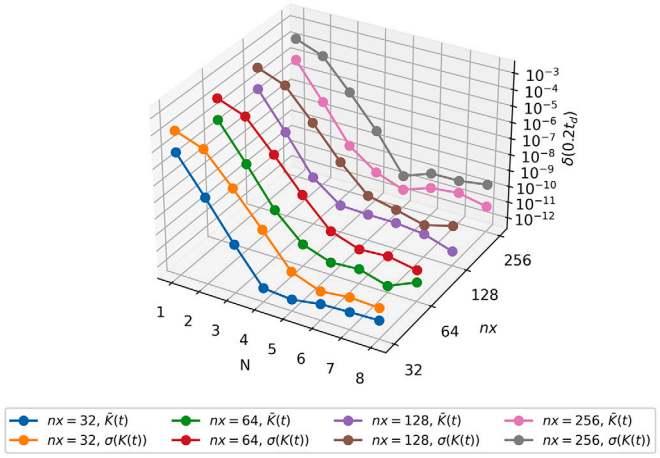

(b) Relative error $(\delta(t))$ at $t = 0.5t_d$

Fig. 1. Relative error $(\delta(t))$ of expectation value $(\bar{K}(t))$ and standard deviation $(\sigma(K(t)))$ of normalized total kinetic energy $K(t)$ for two-dimensional TGV flow computed with SG LBM with respect to highest polynomial order results at different points in time $t = 0.2t_d, 0.5t_d$. Several spatial resolutions $(nx = 32, 64, 128, 256)$ and polynomial orders $(N = 1, 2, 3, \ldots, 8)$ are tested. (For interpretation of the colors in the figure(s), the reader is referred to the web version of this article.)

Table 1
Spatial EOC results of SG LBM in terms of δ (see (81)).

Resolution	8	16	32	64	Order
δ	0.1512	0.04435	0.01104	0.002262	2.02

Here, $\bar{K}_N^{nx}(t)$ represents the total kinetic energy $K(t)$ using polynomial order N with resolution nx.

The results of this EOC study are summarized in Table 1 and plotted in Fig. 2. The linear regression fit validates a second order consistency in space.

Moreover, the EOC study shows that a grid size of 32×32 achieved a relative error of 1% compared to the highest resolution. Consequently, the computational domain was discretized into a grid size of $(nx = ny = 32)$.

For the purpose of comparison, we analyzed the expectation and standard deviation of the velocity component u in the x-direction at $t = 0.5t_d$ and compared it with the results obtained from the MCS for different sample sizes (1E2, 1E3, 1E4). These comparison results, illustrated in Fig. 3, demonstrate the high accuracy achieved by our proposed method with small polynomial orders and a significantly improved convergence rate compared to MCS.

We conducted a comparison of computational time costs among different numerical methods, and the results are presented in Table 2. This study was conducted using an 8-core, 16-thread Intel Core i7-10700KF processor with OpenMP support. For the comparison, we utilized SG LBM with polynomial orders of $N = 5$ and $M = 11$ to simulate the TGV flow with resolution $N = 32$. The number

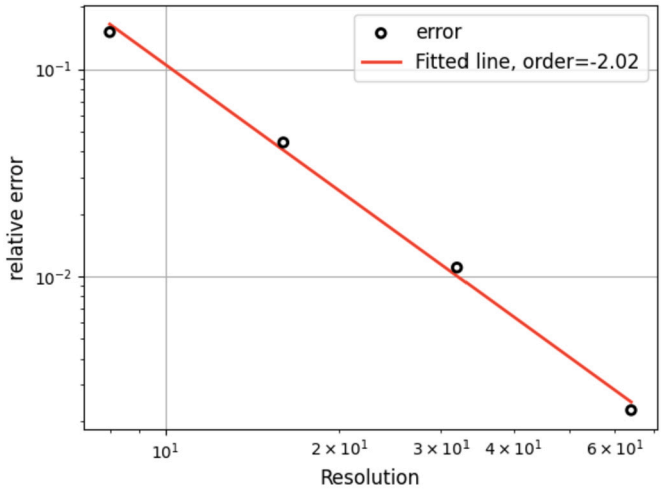

Fig. 2. Spatial EOC results of SG LBM for TGV flow in terms of δ (see (81)).

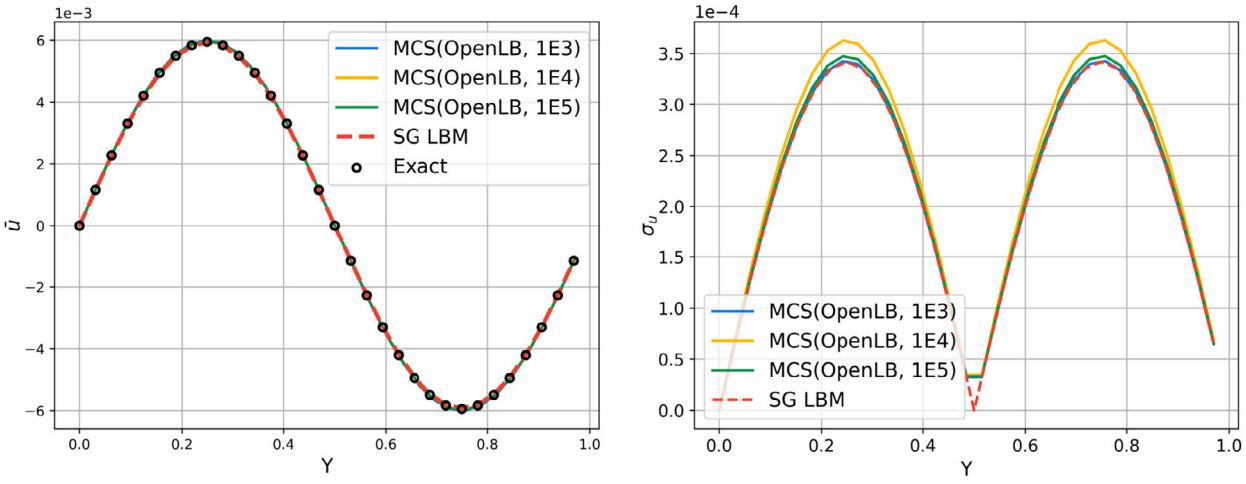

(a) Expectation (b) Standard deviation

Fig. 3. Expectation values ($\bar{u}$) and standard deviations ($\sigma(u)$) of velocity in the x-direction along the central vertical line. Spatial resolution $nx = 32$ and polynomial order $N = 5$ are used.

Table 2
Computational time costs of several numerical methods in seconds for TGV flow.

method	cpu time [s]
SG LBM (OpenMP)	1.02
MC LBM (OpenMP)	341.05
MC LBM (OpenLB, MPI)	240.395

of quadrature points, $M = 2N + 1$, ensures that the gPC provides a robust approximation [62]. Additionally, we implemented MCS on the deterministic LBM part of our SG LBM code as well as on OpenLB. Both MCS employed 10,000 samples to ensure convergence in the TGV flow problem. The results demonstrate that MCS with OpenLB achieves a good speed-up rate (factor eleven) compared to the LBM code without any optimization. Moreover, our proposed SG LBM exhibits a significantly high speed-up rate (factor 334) compared to the MCS LBM.

It is notable that the computational cost of SG LBM is influenced by the resolution, polynomial order, and quadrature points. While the resolution influence is similar to that of the standard LBM, the polynomial order and quadrature points are unique characteristics of SG LBM, and their specific impact remains unknown. Therefore, it is imperative to conduct an analysis of these factors. To ensure sufficient data for an efficiency study, we choose a spatial resolution of $nx = 64$. Subsequently, we investigate the individual influence

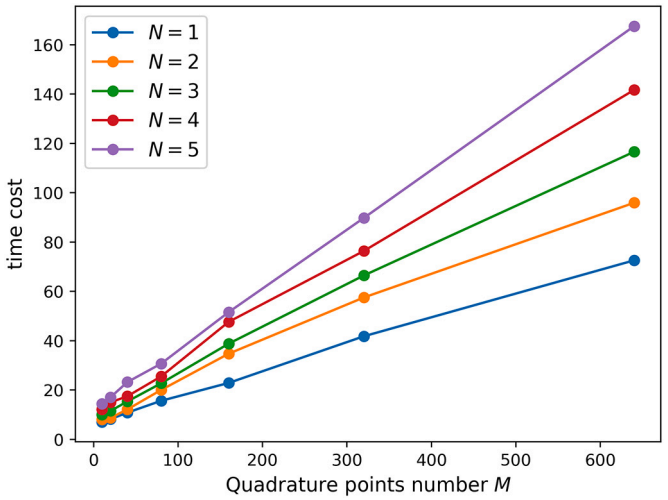

Fig. 4. Influence of number of quadrature points M for different polynomial orders $N = 1, 2, 3, 4, 5$ on time cost of TGV flow simulation with SG LBM at spatial resolution $nx = 64$.

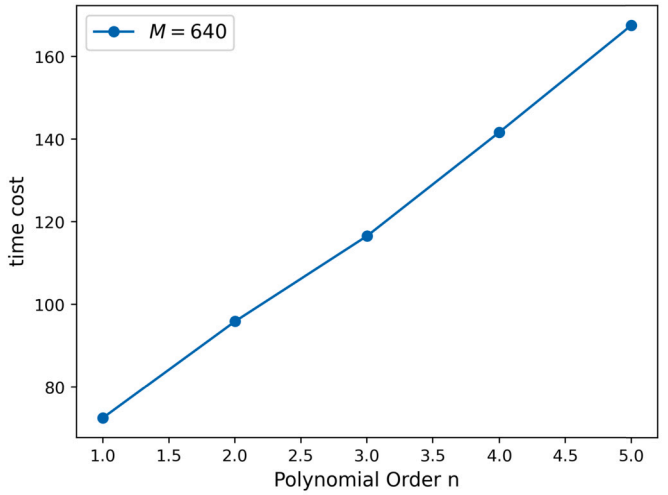

Fig. 5. Influence of polynomial order (tested $n = 1, 2, 3, 4, 5$) with number of quadrature points $M = 640$ on time cost of TGV flow simulation with SG LBM at spatial resolution $nx = 64$.

of polynomial order and quadrature points separately, and the results are presented in Fig. 4 and Fig. 5, respectively. The results demonstrate that both polynomial order and quadrature points exhibit a linear increase in computational cost.

In our analysis, we evaluate and compare the performance of the SG LBM against the MC LBM for simulating TGV flow at $t = 0.5t_d$ on an Intel Xeon Platinum 8368 CPU. This comparative study is conducted across various resolutions to understand the efficiency with respect to consistency of the here used methods in handling stochastic variables. In the implementation of the SG LBM, polynomial orders ranging from 1 to 8 are employed. For the MC LBM, 200 samples are used, with the number of samples denoted as n. The CPU time for 2, 10, and 100 samples is used for comparison. The results (efficiency with respect to consistency), as illustrated in the series of plots in Fig. 6, reveal that the SG LBM exhibits strongly increased consistency orders and reduced computational demand, compared to the MC LBM. The relative error metric used in this comparison is defined as

$$\delta_{\mathrm{SGLBM}} = \frac{\left|\bar{K}_N^{nx} - \bar{K}_8^{nx}\right|}{\left|K_8^{nx}\right|}, \tag{82}$$

$$\delta_{\mathrm{MCLBM}} = \frac{\left|\bar{K}_n^{nx} - \bar{K}_{200}^{nx}\right|}{\left|\bar{K}_{200}^{nx}\right|}. \tag{83}$$

To measure the efficiency with respect to accuracy of SG LBM compared to MC LBM, an experimental speedup analysis is conducted. For the MC LBM, the resolutions $nx = 16, 32, 128, 256$ are used, with samples numbers of $M = 12, 25, 50, 100, 200$, respectively.

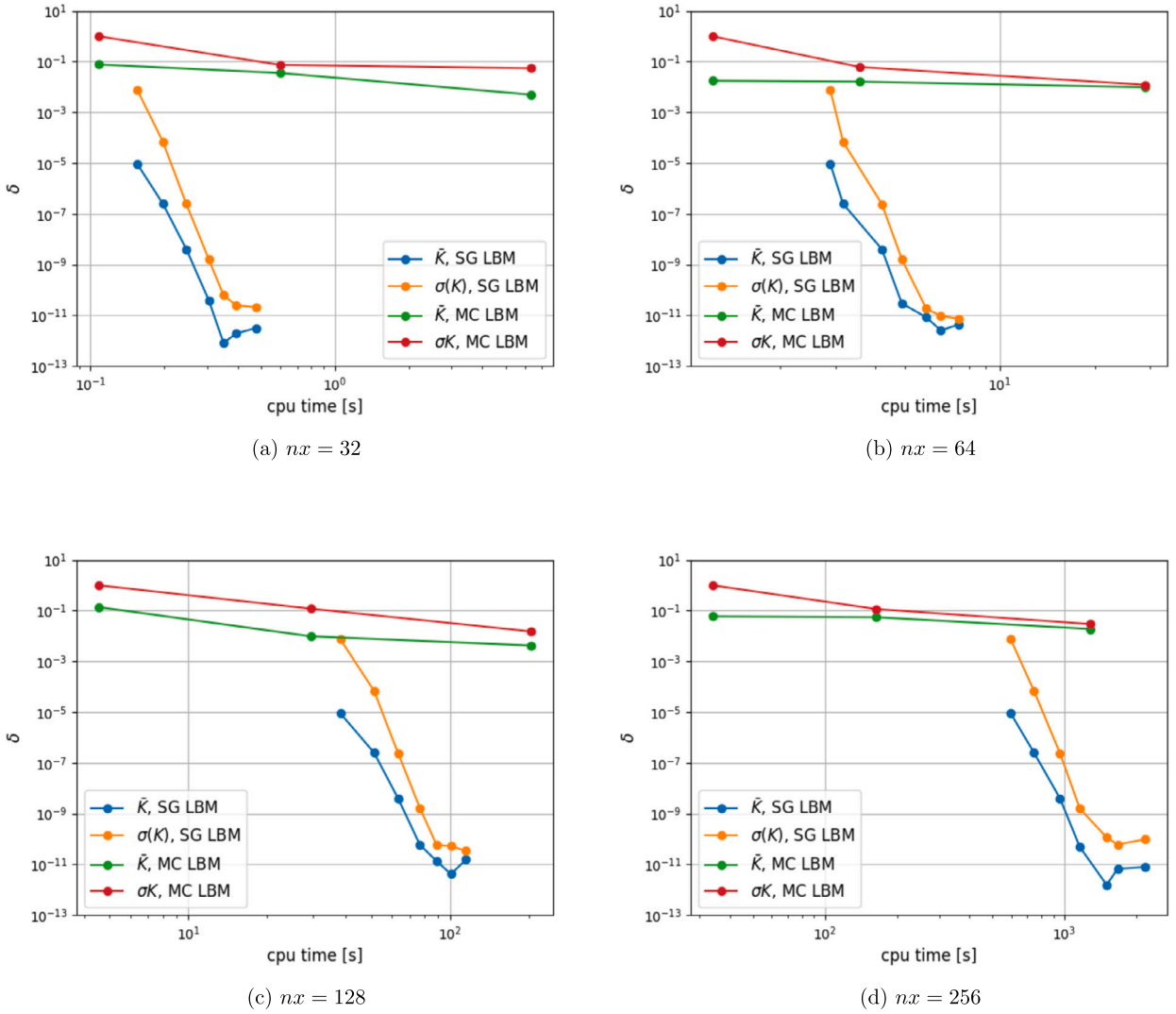

(a) $nx = 32$ (b) $nx = 64$

(c) $nx = 128$ (d) $nx = 256$

Fig. 6. Comparative performance analysis of the SG LBM and MC LBM for the TGV flow at several spatial resolutions $nx = 32, 64, 128, 256$. The error σ is measured in terms of (82) and (83). CPU time in seconds for MC LBM measured for $M = 2, 10, 100$ samples and for SG LBM for polynomial orders from 1 to 8, respectively.

For the SG LBM, polynomial orders $N = 5, 6, 7$ are used. Since exact statistical solutions for a given problem are generally unknown [12], we study accuracy with respect to a highest spatial and stochastic resolution MCS. The converged MC LBM results at resolution $nx = 256$ are considered as the reference solution with a sample number of $M = 60000$. The relative error σ with respect to this reference solution of $\bar{K}$ has been computed as above. The speedup results according to

$$\text{speedup}_{\text{SG}} = \left(\frac{\delta_{\text{MCLBM}}}{\delta_{\text{SGLBM}}} \right)^{\frac{1}{2}} \tag{84}$$

are presented in Fig. 7. On average, our novel SG LBM shows a conventional speedup factor of $\delta_{\text{MCLBM}}/\delta_{\text{SGLBM}} \approx 5.72$.

5.2. Taylor-Green vortex flow with four-dimensional uncertainties

The initial condition of the TGV flow with four-dimensional uncertainties is defined as

$$\boldsymbol{u}(x, y, 0) = \begin{pmatrix} u(x, y, 0) \\ v(x, y, 0) \end{pmatrix} = \begin{pmatrix} -u_0^R \cos(k_x x) \sin(k_y y) \\ u_0^R \sin(k_x x) \cos(k_y y) \end{pmatrix}, \tag{85}$$

$$p(x, y, 0) = -\frac{1}{4}(u_0^R)^2 \left[\cos(2k_x x) + \left(\frac{k_x}{k_y} \right)^2 \cos(2k_y y) \right] + P_0, \tag{86}$$

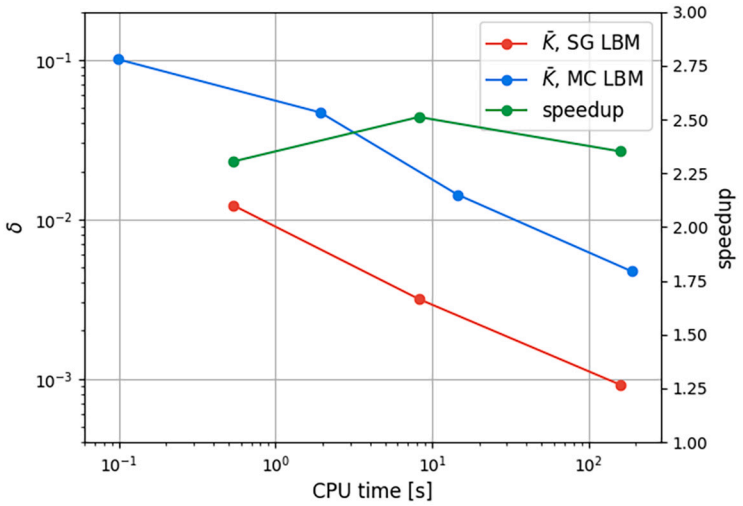

Fig. 7. Speedup analysis of SG LBM (polynomial orders of $N = 5, 6, 7$) compared to MC LBM (resolutions are $nx = 16, 32, 128, 256$ with corresponding sample numbers of $M = 12, 25, 50, 100, 200$) according to (84) measured in terms of to CPU time over accuracy with respect to MC LBM reference solution with resolution $nx = 256$ and $M = 60000$ samples.

where all deterministic parameters are kept the same in the Section 5.1. The difference is that uncertainties are introduced into the velocity $u_0^R = u_0 + \epsilon_d(x)$, where the perturbation ϵ_d is given by the first-order harmonics with four-dimensional i.i.d. uniform distributed random amplitude $\delta_{d,i,j} \sim \mathcal{U}(-0.025, 0.025)$, i.e.

$$\epsilon_d(x, y) = \frac{1}{4} \sum_{(i,j)\in\{0,1\}^2} \delta_{d,i,j} \alpha_i(4x)\alpha_j(4y), \tag{87}$$

where

$$\alpha_i(x) = \begin{cases} \sin(x) & \text{if } i = 0, \\ \cos(x) & \text{if } i = 1. \end{cases} \tag{88}$$

The computational results are shown in Fig. 8 and Fig. 9, demonstrating that the velocity field obtained from the SG LBM are consistent with those from the MC LBM.

For the purpose of comparison, we analyze the expectation and standard deviation of the velocity component u in the x-direction at $t = 0.5t_d$ and compare it with the results obtained from the MC LBM for different sample sizes 1E3, 1E4 and 1E5. These comparison results, illustrated in Fig. 10, demonstrate the higher accuracy achieved by our proposed method compared to MC LBM.

We also evaluate and compare the performance of the SG LBM and the MC LBM on an Intel Xeon Platinum 8368 CPU. In the implementation of the SG LBM, polynomial orders ranging from $N = 1$ to $N = 5$ are used. For the reference MC LBM, 10^6 samples are used. The CPU time for $n = 10, 10^2, 10^3$ samples in MC LBM is used for comparison. The relative error in this comparison is defined as follows:

$$\delta_{\text{SGLBM}} = \frac{\left|\bar{K}_N^{32} - \bar{K}_8^{32}\right|}{\left|\bar{K}_5^{32}\right|}, \tag{89}$$

$$\delta_{\text{MCLBM}} = \frac{\left|\bar{K}_n^{32} - \bar{K}_{100000}^{32}\right|}{\left|\bar{K}_{100000}^{32}\right|}. \tag{90}$$

The results are illustrated in Fig. 11. It is found that both, the expectation $\bar{K}$ and the standard deviation $\sigma(K)$ from the SG LBM converge very quickly, indicating that the TGV flow is not sensitive to this four-dimensional uncertainty in velocity. Although the computational cost of the SG LBM increases exponentially with the number of uncertainties, for the four-dimensional uncertainty case, it remains a superior choice for this test problem compared to the MC LBM.

5.3. Lid-driven cavity flow

The classical incompressible lid-driven cavity (LDC) flow involves a square cavity filled with fluid, where the top wall is driven to move while the other three walls remain stationary. The velocity of the top wall is set to a constant value, denoted as $u_w = 1.0$, and the characteristic length is defined as $L = 1.0$. This case is characterized solely by the Reynolds number $Re = u_w L/\nu = 1000$, which governs the flow behavior. We have chosen a relaxation time of $\tau = 0.5384$ for our simulations.

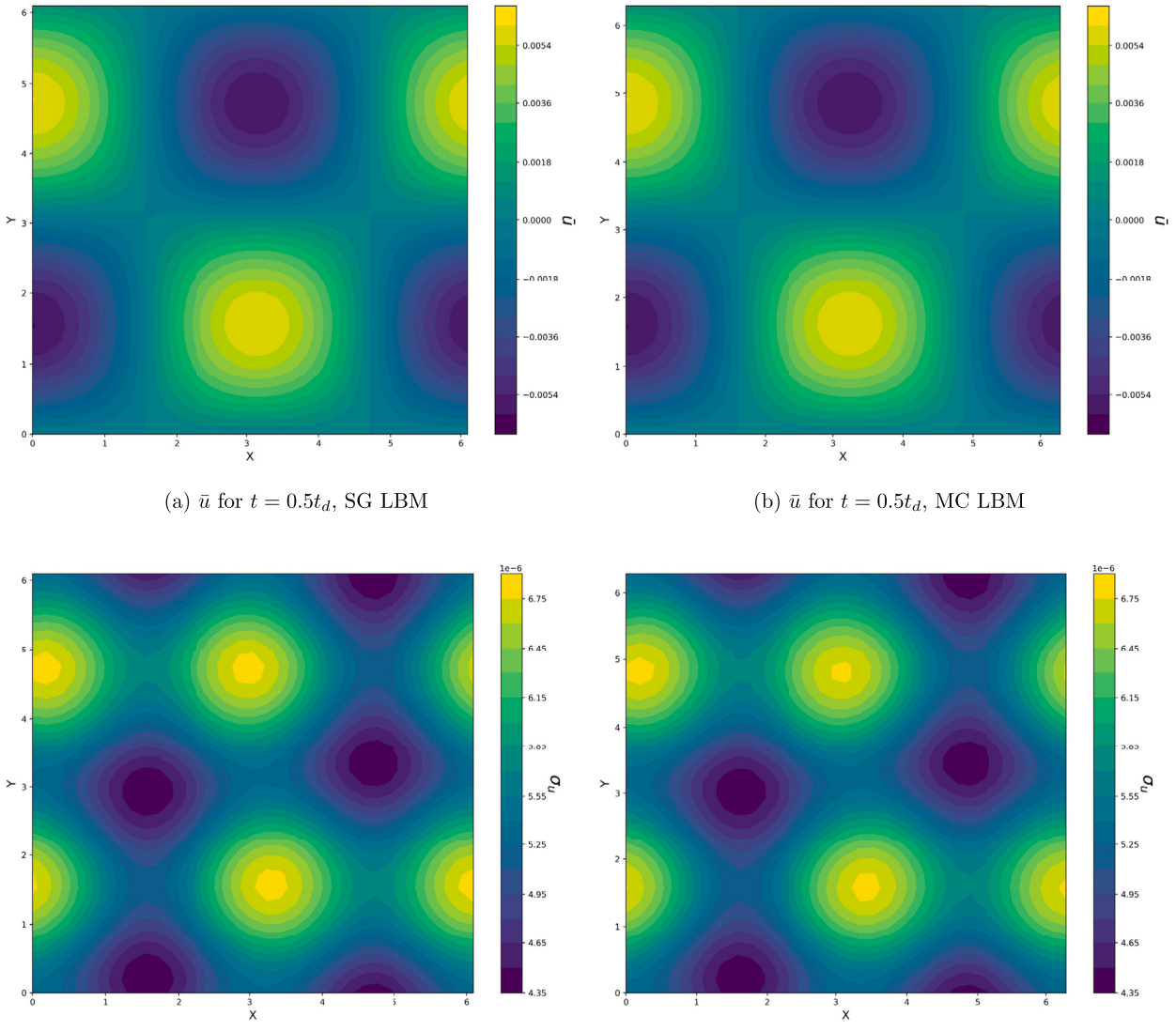

(a) $\bar{u}$ for $t = 0.5t_d$, SG LBM

(b) $\bar{u}$ for $t = 0.5t_d$, MC LBM

(c) σ_u for $t = 0.5t_d$, SG LBM

(d) σ_u for $t = 0.5t_d$, MC LBM

Fig. 8. Expectation values ($\bar{u}$) and standard deviations ($\sigma(u)$) of velocity in the x-direction of TGV flow computed with SG LBM and MC LBM (sample numbers $M = 10000$). Spatial resolution $nx = 33$, polynomial order $N = 3$, and number of quadrature points $M = 7$ are used.

In this test case, we specifically investigate the impact of uncertainty in the boundary condition. By considering the stochastic nature of the driven velocity, we aim to understand how variations in the boundary condition affect the flow behavior and its statistical properties. The stochastic driven velocity is set as $u_w \sim \mathcal{U}_{[0.09,0.11]}$ and we approximate a constant density of $\rho = 1.0$ [63]. To capture the uncertainty in the system, we utilize a polynomial order of $N = 3$ and a set of quadrature points with $M = 7$.

The computational domain in our simulation is discretized into a grid $(x, y) \in [0, nx] \times [0, ny]$. The mean and standard deviation of velocity in the x-direction on a grid $nx = ny = 128$ are shown in Fig. 12.

To enable a comprehensive comparison, we include benchmark solutions from Ghia et al. [64] and results obtained using the MC LBM. Fig. 13 and Fig. 14 illustrate the comparison of the expectation and standard deviation of the velocity in the x-direction along the central vertical line and the y-direction along the central horizontal line, respectively. The results demonstrate that the expectation values of SG LBM approximate the reference result from Ghia et al. [64]. In addition SG LBM exhibits a significantly faster convergence rate compared to the MC LBM (tested for sample sizes 1E3 and 1E4) as indicated by the standard deviations plotted in Figs. 13 and 14.

We investigate the spatial consistency of SG LBM also for the LDC flow. The relative L^2-norm error is measured based on the velocity along the central line, i.e.

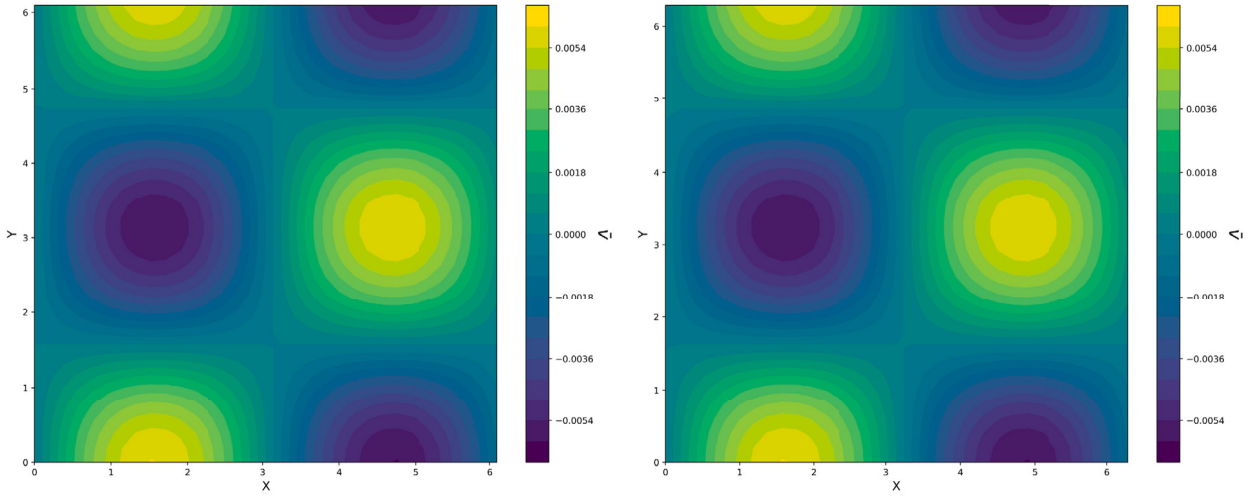

(a) $\bar{v}$ for $t = 0.5t_d$, SG LBM (b) $\bar{v}$ for $t = 0.5t_d$, MC LBM

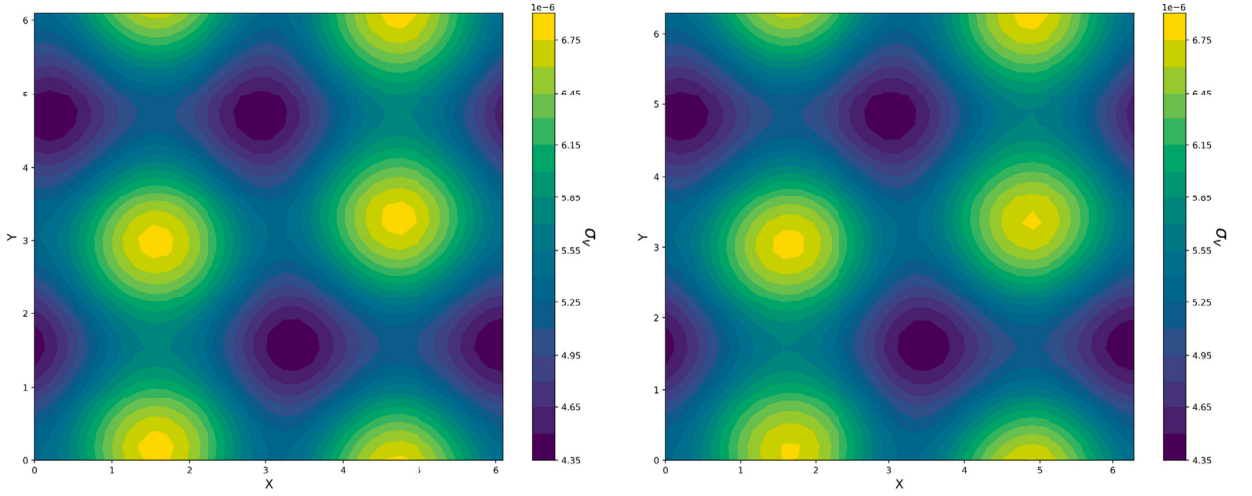

(c) σ_v for $t = 0.5t_d$, SG LBM (d) σ_v for $t = 0.5t_d$, MC LBM

Fig. 9. Expectation values ($\bar{v}$) and standard deviations ($\sigma(v)$) of velocity in the y-direction of TGV flow computed with SG LBM and MC LBM (sample numbers $M = 10000$). Spatial resolution $nx = 33$, polynomial order $N = 3$, and number of quadrature points $M = 7$ are used.

$$\delta_2 = \left\| \left(\frac{\left| \bar{\boldsymbol{u}}_3^{nx} - \bar{\boldsymbol{u}}_3^{512} \right|}{\left| \bar{\boldsymbol{u}}_3^{512} \right|} \right) \right\|_2 , \tag{91}$$

and plotted in Fig. 15. As expected, the results reveal a second order convergence rate in space.

The stochastic consistency is also investigated for several resolutions based on δ (see (79) with respect to u-velocity). The results are shown in Fig. 16, which shows that unlike the TGV flow, the LDC flow requires a higher polynomial order to converge. However, the spectral convergence rate is also numerically approved for the LDC flow. In case of a polynomial order $N = 8$, the results reach machine precision.

5.4. Isentropic vortex convection

As a last test case, the isentropic vortex convection (IVC) by an inviscid uniform flow with a free-stream Mach number of $Ma = 0.042$ ($u_\infty = 0.05$) is simulated. The computational domain has dimensions of $[0, 10] \times [0, 10]$ and is discretized into a 100×100 uniform grid. The characteristic length $L = 10$, the voxel length $dx = 0.1$. The periodic boundary condition is applied to all boundaries of the domain [65]. The viscosity is set as $\nu = 10^{-15}$, which leads to a very large Reynolds number $\mathrm{Re} = 5 \times 10^{14}$. We have chosen a

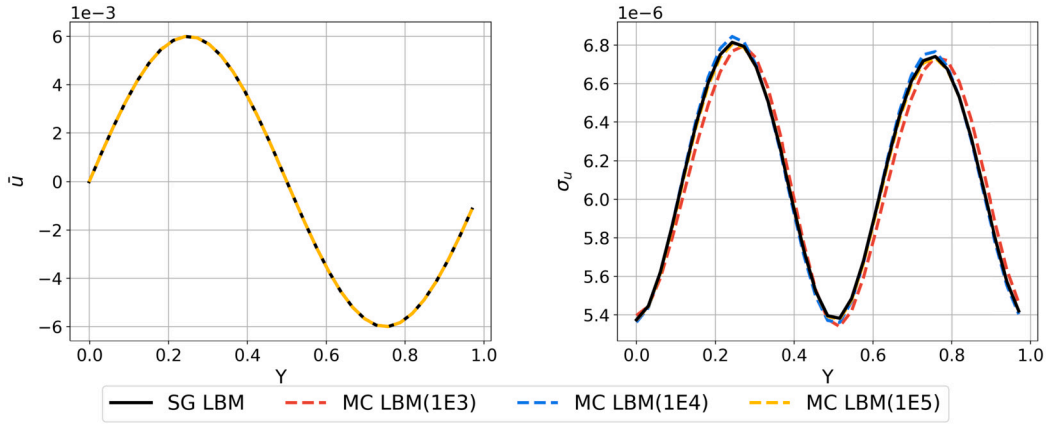

Fig. 10. Expectation values $\bar{u}$ (left) and standard deviations ($\sigma(u)$) (right) of velocity in the x-direction along the central vertical line computed with MC LBM for sample sizes 1E3, 1E4, 1E5 and with SG LBM. The spatial resolution is $nx = 32$ and for SG LBM a polynomial order $N = 3$ and $M = 7$ quadrature points are used.

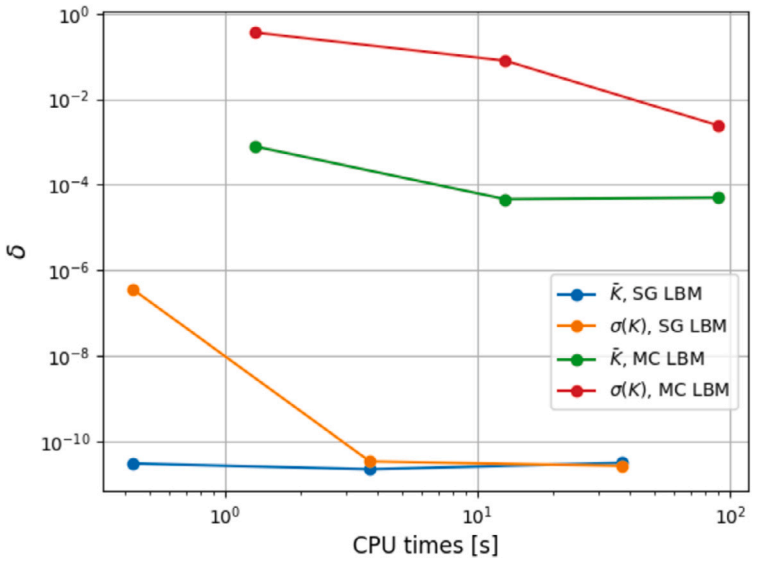

(a)

Fig. 11. Comparative performance analysis of the SG LBM and MC LBM for the TGV flow with spatial resolution $nx = 32$ and four-dimensional uncertainties. The error σ is measured in terms of (82) and (83). CPU time in seconds for MC LBM measured for $M = 10, 100, 1000$ samples and for SG LBM for polynomial orders from 1 to 4, respectively.

relaxation time of $\tau = \nu/C_s^2 + 0.5$. The IVC is used to show that SG LBM accurately captures vortical flows. Several conditions are set, specifically

$$\rho_\infty = 1.0, \quad u_\infty = 0.05\xi, \quad v_\infty = 0.0, \tag{92}$$

where ξ is the uncertainty parameter and follows a uniform distribution $\xi \sim \mathcal{U}_{[0.9,1.1]}$. Based on that, perturbations are introduced to the free-stream flow, given by

$$\rho = \left[1 - \frac{(\gamma-1)\,b^2}{8\gamma\pi^2}\exp\left(1-r^2\right)\right]^{\frac{1}{\gamma-1}}, \tag{93}$$

$$u = u_\infty - \frac{b}{2\pi}\exp\left(\frac{1}{2}\left(1-r^2\right)\right)\left(y-y_c\right), \tag{94}$$

$$v = v_\infty - \frac{b}{2\pi}\exp\left(\frac{1}{2}\left(1-r^2\right)\right)\left(x-x_c\right), \tag{95}$$

where $b = 0.05$ represents the vortex strength, and $r = \sqrt{(x-x_c)^2 + (y-y_c)^2}$ is the distance from the vortex center located at $(x_c, y_c) = (5, 5)$.

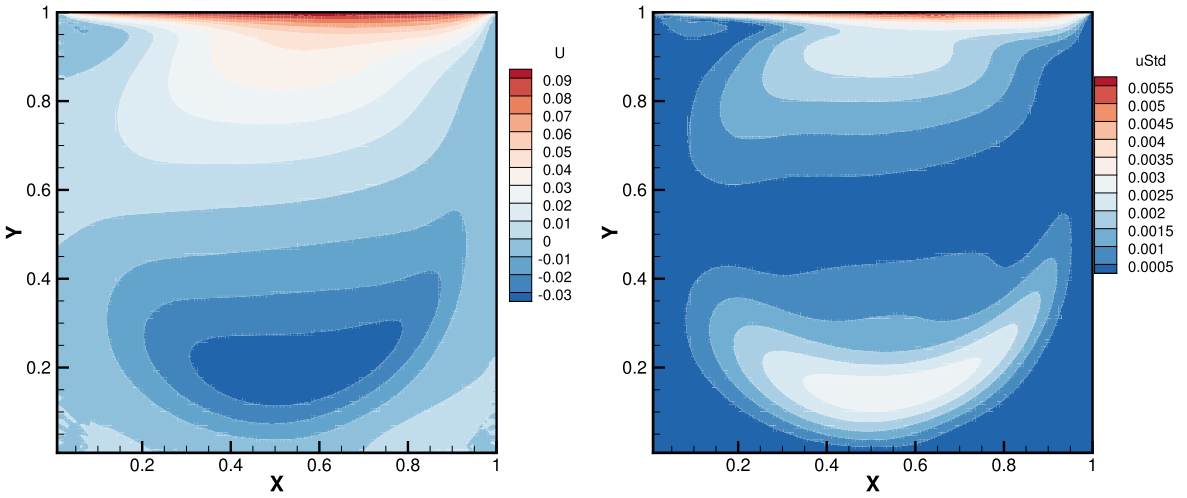

(a) Expectation values ($\bar{u}$) (b) Standard deviation ($\sigma(u)$)

Fig. 12. Expectation values ($\bar{u}$) and standard deviations ($\sigma(u)$) of velocity in the x-direction of LDC flow computed with SG LBM. Spatial resolution $nx = 128$, polynomial order $N = 3$, and number of quadrature points $M = 7$ are used.

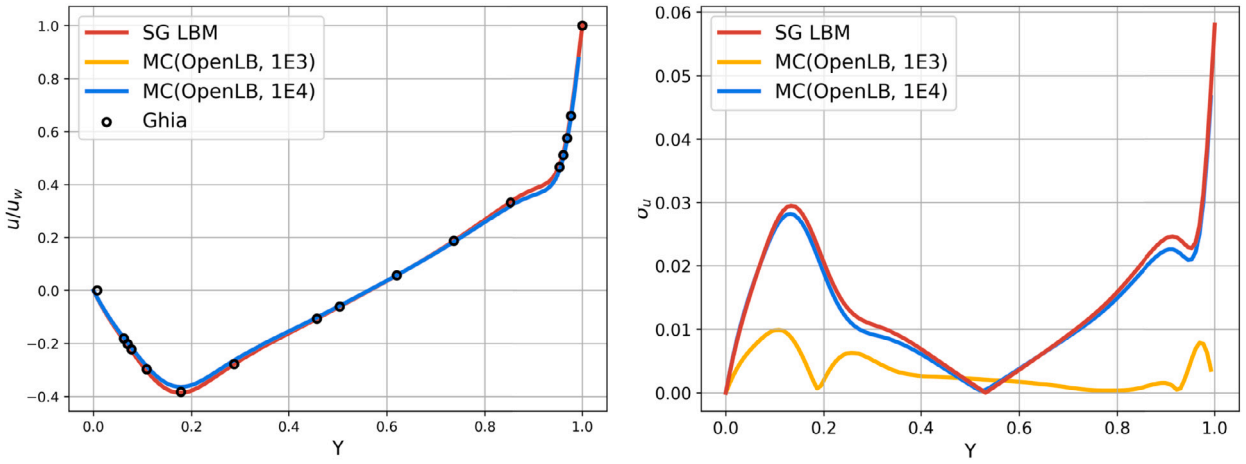

(a) Expectation (b) Standard deviation

Fig. 13. Expectation values ($\bar{u}$) and standard deviations ($\sigma(u)$) of velocity in the x-direction along the central vertical line of LDC flow computed with SG LBM. Spatial resolution $nx = 128$, polynomial order $N = 3$, and number of quadrature points $M = 7$ are used.

To capture the uncertainty in the system, we utilize a polynomial order of $N = 4$ and a set of quadrature points with $M = 9$. The velocity profile is extracted from the flow field evolved for 20 flow-through-times (FFTs) Fig. 17 shows the expectation values and standard deviation specifically at $t = 20$FFTs. The SG LBM results for approximating inviscid flows show good agreement to the exact prediction as well as to the MCS LBM (OpenLB) results.

6. Conclusion

In conclusion, by decomposing the LBE into polynomials and employing the Galerkin projection, we have first implemented the Stochastic Galerkin method on the conventional lattice Boltzmann equation. This work aims to address the need for a more efficient and accurate UQ method in CFD problems.

Our numerical results, obtained through simulations of Taylor-Green vortex flow, lid-driven cavity flow, and isentropic vortex convection, showcased the accuracy and computational efficiency of the SG LBM approach. The comparison with MC LBM as a benchmark demonstrated the superior convergence rate and smaller computational cost of SG LBM. Compared to MC LBM the novel SG LBM reaches a speedup factor of 5.72 on average in a randomized two-dimensional Taylor–Green vortex flow test case.

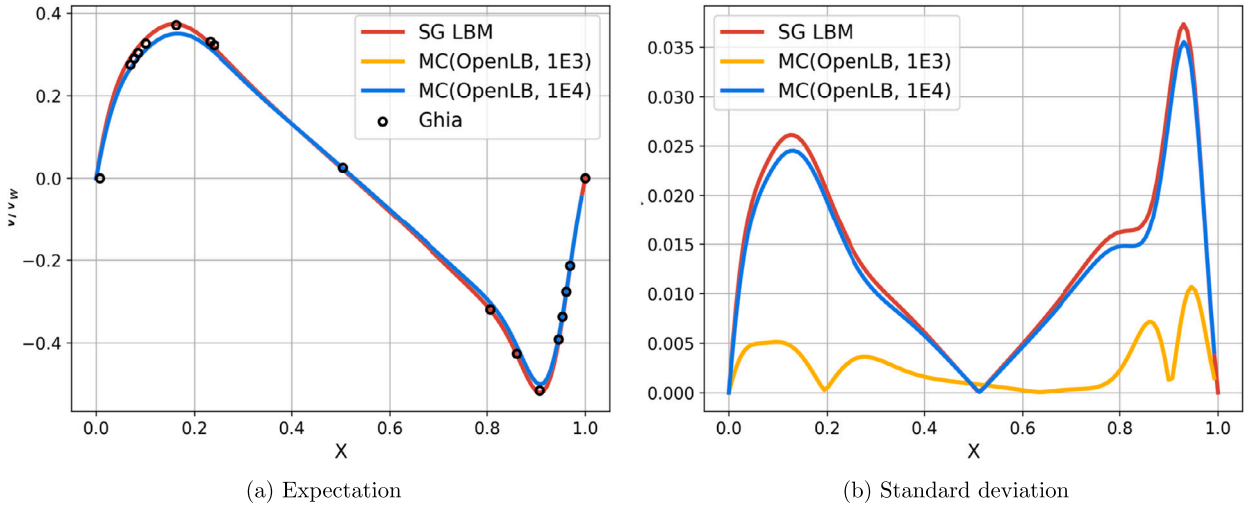

Fig. 14. Expectation values ($\bar{u}$) and standard deviations ($\sigma(u)$) of velocity in the y-direction along the central horizontal line of LDC flow computed with SG LBM. Spatial resolution $nx = 128$, polynomial order $N = 3$, and number of quadrature points $M = 7$ are used.

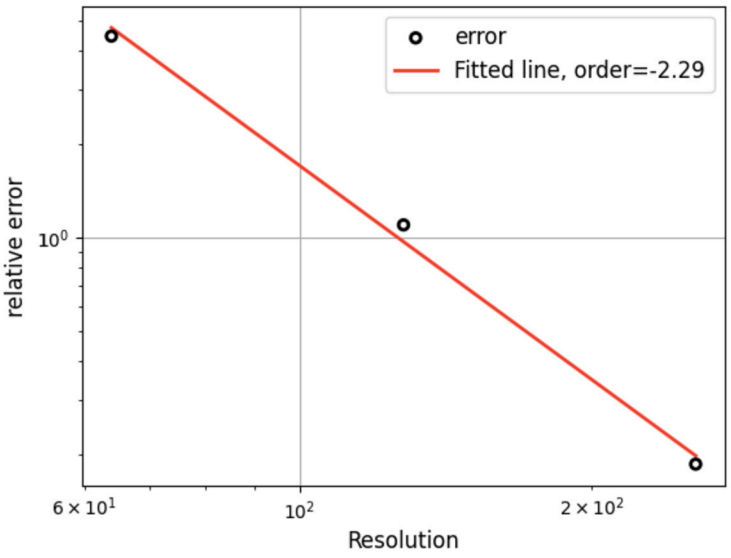

Fig. 15. Spatial EOC results of SG LBM for LDC flow in terms of δ_2 (see (91)).

Overall, our study highlights the potential of the SG LBM as an intrusive UQ technique for UQ in CFD simulations. The combination of high efficiency, accuracy, and computational effectiveness makes SG LBM a valuable tool for addressing uncertainties arising from various sources in CFD.

CRediT authorship contribution statement

Mingliang Zhong: Writing – original draft, Visualization, Software, Methodology, Investigation, Formal analysis, Data curation. **Tianbai Xiao:** Writing – review & editing, Supervision. **Mathias J. Krause:** Supervision, Software, Funding acquisition, Conceptualization. **Martin Frank:** Supervision, Resources, Funding acquisition, Conceptualization. **Stephan Simonis:** Writing – review & editing, Writing – original draft, Visualization, Validation, Supervision, Project administration, Methodology, Formal analysis, Data curation, Conceptualization.

Declaration of competing interest

The authors declare that they have no known competing financial interests or personal relationships that could have appeared to influence the work reported in this paper.

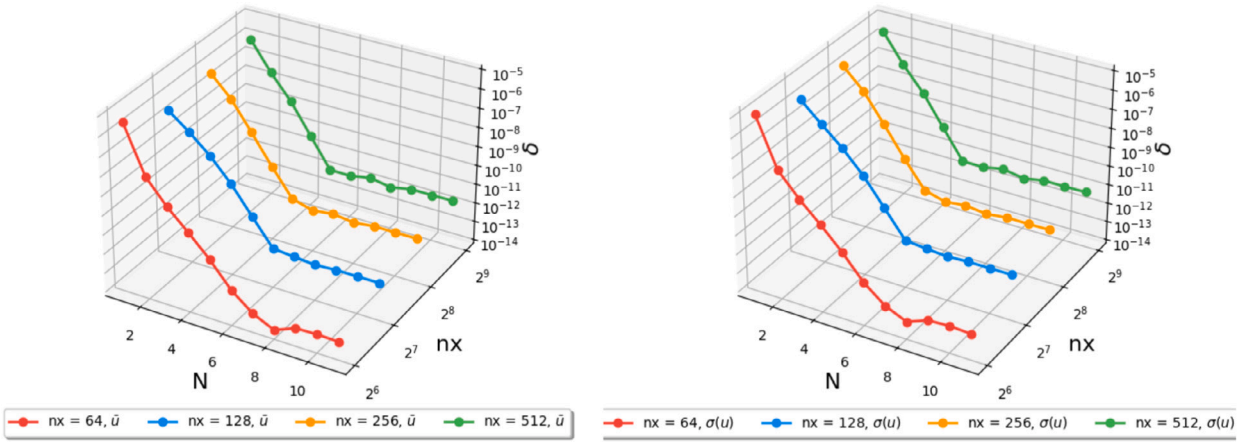

(a) Expectation (b) Standard deviation

Fig. 16. Relative error (δ, see (79)) of expectation value ($\bar{u}$) and standard deviation ($\sigma(u)$) of u-velocity along the central vertical line of LDC flow computed with SG LBM. Several spatial resolutions ($nx = 64, 128, 256, 512$) and polynomial orders ($N = 1, 2, 3, \ldots, 13$) are tested.

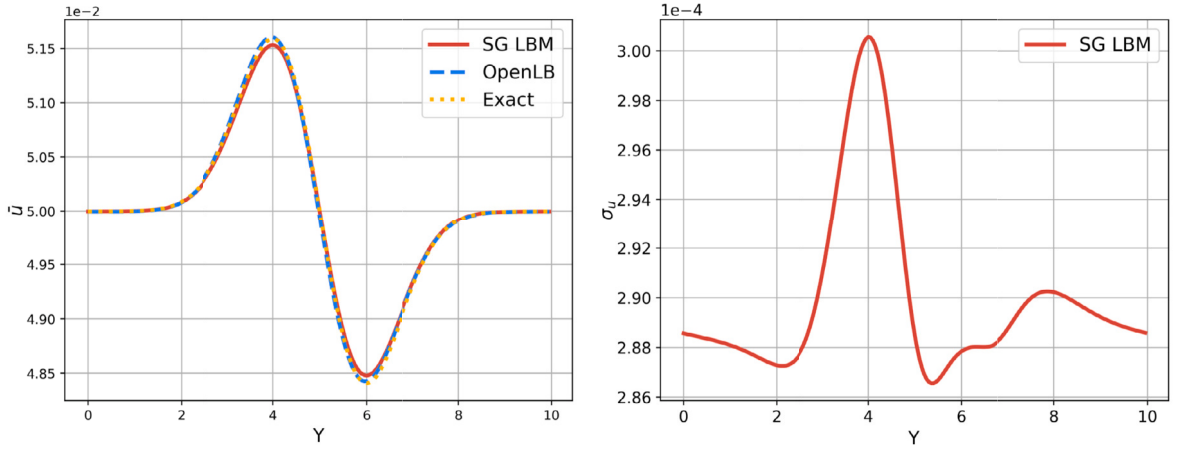

(a) Expectation (b) Standard deviation

Fig. 17. Expectation values ($\bar{u}$) and standard deviations ($\sigma(u)$) of velocity in the y-direction along the central horizontal line of IVC computed with SG LBM. Spatial resolution $nx = 100$, polynomial order $N = 4$, and $M = 9$ quadrature points are tested. MCS LBM (OpenLB) results and an exact prediction are plotted as a reference.

Data availability

Parts of present results have been produced with the open source C++ LBM library OpenLB (www.openlb.net). The generated data are available from the authors upon reasonable request.

Acknowledgement

The authors thank the reviewers for the insightful comments that considerably improved this manuscript. This work was performed on the HoreKa supercomputer funded by the Ministry of Science, Research and the Arts Baden-Württemberg and by the Federal Ministry of Education and Research. This work was partly funded by the "Deutsche Forschungsgemeinschaft" (DFG, German Research Foundation), project number 436212129. Tianbai Xiao acknowledges the financial support of the National Science Foundation of China (No. 12302381).

References

[1] T.A. Oliver, R.D. Moser, Bayesian uncertainty quantification applied to rans turbulence models, J. Phys. Conf. Ser. 318 (2011) 042032, IOP Publishing.
[2] H. Wang, D.A. Sheen, Combustion kinetic model uncertainty quantification, propagation and minimization, Prog. Energy Combust. Sci. 47 (2015) 1–31.
[3] R.C. Smith, Uncertainty Quantification: Theory, Implementation, and Applications, vol. 12, SIAM, 2013.
[4] T.J. Sullivan, Introduction to Uncertainty Quantification, vol. 63, Springer, 2015.

[5] H.N. Najm, Uncertainty quantification and polynomial chaos techniques in computational fluid dynamics, Annu. Rev. Fluid Mech. 41 (2009) 35–52, https://doi.org/10.1146/annurev.fluid.010908.165248.
[6] D. Lucor, C. Enaux, H. Jourdren, P. Sagaut, Stochastic design optimization: application to reacting flows, Comput. Methods Appl. Mech. Eng. 196 (49–52) (2007) 5047–5062, https://doi.org/10.1016/j.cma.2007.07.003.
[7] W.J. Morokoff, R.E. Caflisch, Quasi-Monte Carlo integration, J. Comput. Phys. 122 (2) (1995) 218–230, https://doi.org/10.1006/jcph.1995.1209.
[8] M.B. Giles, Multilevel Monte Carlo methods, Acta Numer. 24 (2015) 259–328, https://doi.org/10.1017/S096249291500001X.
[9] D. Xiu, Numerical Methods for Stochastic Computations: A Spectral Method Approach, Princeton University Press, 2010.
[10] F. Leonardi, S. Mishra, C. Schwab, Numerical approximation of statistical solutions of planar, incompressible flows, Math. Models Methods Appl. Sci. 26 (13) (2016) 2471–2523, https://doi.org/10.1142/S0218202516500597.
[11] U.S. Fjordholm, K. Lye, S. Mishra, Numerical approximation of statistical solutions of scalar conservation laws, SIAM J. Numer. Anal. 56 (5) (2018) 2989–3009, https://doi.org/10.1137/17M1154874.
[12] P. Bansal, Numerical approximation of statistical solutions of the incompressible Navier-Stokes equations, arXiv preprint, https://doi.org/10.48550/ARXIV.2107.06073, https://arxiv.org/abs/2107.06073, 2021.
[13] S. Lanthaler, S. Mishra, C. Parés-Pulido, Statistical solutions of the incompressible Euler equations, Math. Models Methods Appl. Sci. 31 (02) (2021) 223–292, https://doi.org/10.1142/S0218202521500068.
[14] L. Mathelin, M.Y. Hussaini, T.A. Zang, Stochastic approaches to uncertainty quantification in CFD simulations, Numer. Algorithms 38 (1) (2005) 209–236, https://doi.org/10.1007/BF02810624.
[15] D. Xiu, J.S. Hesthaven, High-order collocation methods for differential equations with random inputs, SIAM J. Sci. Comput. 27 (3) (2005) 1118–1139, https://doi.org/10.1137/040615201.
[16] I. Babuška, F. Nobile, R. Tempone, A stochastic collocation method for elliptic partial differential equations with random input data, SIAM J. Numer. Anal. 45 (3) (2007) 1005–1034, https://doi.org/10.1137/100786356.
[17] D. Xiu, G.E. Karniadakis, Modeling uncertainty in flow simulations via generalized polynomial chaos, J. Comput. Phys. 187 (1) (2003) 137–167, https://doi.org/10.1016/S0021-9991(03)00092-5.
[18] D. Gottlieb, D. Xiu, Galerkin method for wave equations with uncertain coefficients, Commun. Comput. Phys. 3 (2) (2008) 505–518.
[19] S. Jin, J.-G. Liu, Z. Ma, Uniform spectral convergence of the stochastic Galerkin method for the linear transport equations with random inputs in diffusive regime and a micro–macro decomposition-based asymptotic-preserving method, Res. Math. Sci. 4 (1) (2017) 15, https://doi.org/10.1186/s40687-017-0105-1.
[20] T. Xiao, M. Frank, A stochastic kinetic scheme for multi-scale flow transport with uncertainty quantification, J. Comput. Phys. 437 (2021) 110337, https://doi.org/10.1016/j.jcp.2021.110337.
[21] T. Xiao, M. Frank, A stochastic kinetic scheme for multi-scale plasma transport with uncertainty quantification, J. Comput. Phys. 432 (2021) 110139, https://doi.org/10.1016/j.jcp.2021.110139.
[22] D. Xiu, G.E. Karniadakis, Modeling uncertainty in steady state diffusion problems via generalized polynomial chaos, Comput. Methods Appl. Mech. Eng. 191 (43) (2002) 4927–4948.
[23] P. Delgado, V. Kumar, A stochastic Galerkin approach to uncertainty quantification in poroelastic media, in: Fluids Engineering Division Summer Meeting, vol. 46247, American Society of Mechanical Engineers, 2014, p. V01DT40A002.
[24] A. Medaglia, L. Pareschi, M. Zanella, Stochastic Galerkin particle methods for kinetic equations of plasmas with uncertainties, J. Comput. Phys. 479 (2023) 112011.
[25] S. Succi, The Lattice Boltzmann Equation: for Fluid Dynamics and Beyond, Oxford University Press, 2001.
[26] M. Junk, A. Klar, L.-S. Luo, Asymptotic analysis of the lattice Boltzmann equation, J. Comput. Phys. 210 (2) (2005) 676–704, https://doi.org/10.1016/j.jcp.2005.05.003.
[27] P. Lallemand, L.-S. Luo, M. Krafczyk, W.-A. Yong, The lattice Boltzmann method for nearly incompressible flows, J. Comput. Phys. 431 (2021) 109713, https://doi.org/10.1016/j.jcp.2020.109713.
[28] Z. Guo, C. Shu, Lattice Boltzmann Method and Its Application in Engineering, vol. 3, World Scientific, 2013.
[29] S. Simonis, D. Oberle, M. Gaedtke, P. Jenny, M.J. Krause, Temporal large eddy simulation with lattice Boltzmann methods, J. Comput. Phys. 454 (2022) 110991, https://doi.org/10.1016/j.jcp.2022.110991.
[30] N. Hafen, A. Dittler, M.J. Krause, Simulation of particulate matter structure detachment from surfaces of wall-flow filters applying lattice Boltzmann methods, Comput. Fluids 239 (2022) 105381, https://doi.org/10.1016/j.compfluid.2022.105381.
[31] P. Lallemand, L.-S. Luo, Lattice Boltzmann method for moving boundaries, J. Comput. Phys. 184 (2) (2003) 406–421, https://doi.org/10.1016/S0021-9991(02)00022-0.
[32] R. Mei, L.-S. Luo, W. Shyy, An accurate curved boundary treatment in the lattice Boltzmann method, J. Comput. Phys. 155 (2) (1999) 307–330, https://doi.org/10.1006/jcph.1999.6334.
[33] M. Zhong, S. Zou, D. Pan, C. Zhuo, C. Zhong, A simplified discrete unified gas kinetic scheme for incompressible flow, Phys. Fluids 32 (9) (2020) 093601, https://doi.org/10.1063/5.0021332.
[34] R. Trunk, T. Weckerle, N. Hafen, G. Thäter, H. Nirschl, M.J. Krause, Revisiting the homogenized lattice Boltzmann method with applications on particulate flows, Computation 9 (2) (2021), https://doi.org/10.3390/computation9020011.
[35] S. Simonis, N. Hafen, J. Jeßberger, D. Dapelo, G. Thäter, M.J. Krause, Homogenized lattice Boltzmann methods for fluid flow through porous media – part I: kinetic model derivation, arXiv preprint, https://doi.org/10.48550/arXiv.2310.14746, https://arxiv.org/abs/2310.14746, 2023.
[36] A. Kummerländer, M. Dorn, M. Frank, M.J. Krause, Implicit propagation of directly addressed grids in lattice Boltzmann methods, Concurr. Comput. e7509 (2022), https://doi.org/10.1002/cpe.7509.
[37] A. Kummerländer, F. Bukreev, S. Berg, M. Dorn, M.J. Krause, Advances in computational process engineering using lattice Boltzmann methods on high performance computers for solving fluid flow problems, in: High Performance Computing in Science and Engineering '22, Springer, 2023, https://doi.org/10.1007/978-3-031-46870-4_16.
[38] A. Kummerländer, S. Avis, H. Kusumaatmaja, F. Bukreev, M. Crocoll, D. Dapelo, N. Hafen, S. Ito, J. Jeßberger, J.E. Marquardt, J. Mödl, T. Pertzel, F. Prinz, F. Raichle, M. Schecher, S. Simonis, D. Teutscher, M.J. Krause, OpenLB Release 1.6: Open Source Lattice Boltzmann Code (Apr. 2023), https://doi.org/10.5281/zenodo.7773497.
[39] M. Krause, A. Kummerländer, S. Avis, H. Kusumaatmaja, D. Dapelo, F. Klemens, M. Gaedtke, N. Hafen, A. Mink, R. Trunk, J. Marquardt, M. Maier, M. Haussmann, S. Simonis, OpenLB–Open source lattice Boltzmann code, Comput. Math. Appl. 81 (2021) 258–288, https://doi.org/10.1016/j.camwa.2020.04.033.
[40] S. Simonis, M. Haussmann, L. Kronberg, W. Dörfler, M.J. Krause, Linear and brute force stability of orthogonal moment multiple-relaxation-time lattice Boltzmann methods applied to homogeneous isotropic turbulence, Philos. Trans. R. Soc. A 379 (2021) 20200405, https://doi.org/10.1098/rsta.2020.0405.
[41] S. Simonis, M. Frank, M.J. Krause, Constructing relaxation systems for lattice Boltzmann methods, Appl. Math. Lett. 137 (2023) 108484, https://doi.org/10.1016/j.aml.2022.108484.
[42] S. Simonis, Lattice Boltzmann Methods for Partial Differential Equations, Ph.D. thesis, Karlsruhe Institute of Technology (KIT), 2023.
[43] D. Dapelo, S. Simonis, M.J. Krause, J. Bridgeman, Lattice-Boltzmann coupled models for advection–diffusion flow on a wide range of Péclet numbers, J. Comput. Sci. 51 (2021) 101363, https://doi.org/10.1016/j.jocs.2021.101363.
[44] S. Simonis, J. Nguyen, S.J. Avis, W. Dörfler, M.J. Krause, Binary fluid flow simulations with free energy lattice Boltzmann methods, Discrete Contin. Dyn. Syst., Ser. S (2023), https://doi.org/10.3934/dcdss.2023069.

[45] A. Mink, K. Schediwy, C. Posten, H. Nirschl, S. Simonis, M.J. Krause, Comprehensive computational model for coupled fluid flow, mass transfer, and light supply in tubular photobioreactors equipped with glass sponges, Energies 15 (20) (2022), https://doi.org/10.3390/en15207671.
[46] F. Bukreev, S. Simonis, A. Kummerländer, J. Jeßberger, M.J. Krause, Consistent lattice Boltzmann methods for the volume averaged Navier–Stokes equations, J. Comput. Phys. 490 (2023) 112301, https://doi.org/10.1016/j.jcp.2023.112301.
[47] M. Haussmann, P. Reinshaus, S. Simonis, H. Nirschl, M.J. Krause, Fluid–structure interaction simulation of a Coriolis mass flowmeter using a lattice Boltzmann method, Fluids 6 (4) (2021) 167, https://doi.org/10.3390/fluids6040167.
[48] S. Simonis, M.J. Krause, Forschungsnahe Lehre unter Pandemiebedingungen, Mitt. Dtsch. Math.-Ver. 30 (1) (2022) 43–45, https://doi.org/10.1515/dmvm-2022-0015.
[49] M. Siodlaczek, M. Gaedtke, S. Simonis, M. Schweiker, N. Homma, M.J. Krause, Numerical evaluation of thermal comfort using a large eddy lattice Boltzmann method, Build. Environ. 192 (2021) 107618, https://doi.org/10.1016/j.buildenv.2021.107618.
[50] S. Simonis, S. Mishra, Computing statistical Navier–Stokes solutions, in: R. Abgrall, M. Garavello, M. Lukáčová-Medvid'ová, K. Trivisa (Eds.), Hyperbolic Balance Laws: Interplay Between Scales and Randomness, Oberwolfach Report 10, EMS Press, 2024.
[51] S. Fu, R. So, W.W.F. Leung, Stochastic finite difference lattice Boltzmann method for steady incompressible viscous flows, J. Comput. Phys. 229 (17) (2010) 6084–6103, https://doi.org/10.1016/j.jcp.2010.04.041.
[52] W. Zhao, J. Huang, W.-A. Yong, Lattice Boltzmann method for stochastic convection-diffusion equations, SIAM/ASA J. Uncertain. Quantificat. 9 (2) (2021) 536–563, https://doi.org/10.1137/19M1270665.
[53] L.M. van den Bos, B. Koren, R.P. Dwight, Non-intrusive uncertainty quantification using reduced cubature rules, J. Comput. Phys. 332 (2017) 418–445, https://doi.org/10.1016/j.jcp.2016.12.011.
[54] J. Jacob, L. Merlier, F. Marlow, P. Sagaut, Lattice Boltzmann method-based simulations of pollutant dispersion and urban physics, Atmosphere 12 (7) (2021) 833, https://doi.org/10.3390/atmos12070833.
[55] P. Wang, H. Chen, X. Meng, X. Jiang, D. Xiu, X. Yang, Uncertainty quantification on the macroscopic properties of heterogeneous porous media, Phys. Rev. E 98 (3) (2018) 033306, https://doi.org/10.1103/PhysRevE.98.033306.
[56] P.L. Bhatnagar, E.P. Gross, M. Krook, A model for collision processes in gases. I. Small amplitude processes in charged and neutral one-component systems, Phys. Rev. 94 (1954) 511–525, https://doi.org/10.1103/PhysRev.94.511.
[57] S. Simonis, M.J. Krause, Limit consistency of lattice Boltzmann equations, arXiv preprint, https://doi.org/10.48550/arXiv.2208.06867, https://arxiv.org/abs/2208.06867, 2022.
[58] J. Kusch, R.G. McClarren, M. Frank, Filtered stochastic Galerkin methods for hyperbolic equations, J. Comput. Phys. 403 (2020) 109073.
[59] K. Timm, H. Kusumaatmaja, A. Kuzmin, O. Shardt, G. Silva, E. Viggen, The Lattice Boltzmann Method: Principles and Practice, Springer International Publishing AG, Cham, Switzerland, 2016.
[60] G. Zhao-Li, Z. Chu-Guang, S. Bao-Chang, Non-equilibrium extrapolation method for velocity and pressure boundary conditions in the lattice Boltzmann method, Chin. Phys. 11 (4) (2002) 366, https://doi.org/10.1088/1009-1963/11/4/310.
[61] R. Mei, L.-S. Luo, P. Lallemand, D. d'Humières, Consistent initial conditions for lattice Boltzmann simulations, Comput. Fluids 35 (8–9) (2006) 855–862, https://doi.org/10.1016/j.compfluid.2005.08.008.
[62] S. Hosder, R. Walters, M. Balch, Efficient sampling for non-intrusive polynomial chaos applications with multiple uncertain input variables, in: 48th AIAA/ASME/ASCE/AHS/ASC Structures, Structural Dynamics, and Materials Conference, 2011, p. 1939.
[63] T. Xiao, An investigation of uncertainty propagation in non-equilibrium flows, Int. J. Comput. Fluid Dyn. 36 (4) (2022) 294–318, https://doi.org/10.1080/10618562.2022.2104262.
[64] U. Ghia, K.N. Ghia, C. Shin, High-re solutions for incompressible flow using the Navier-Stokes equations and a multigrid method, J. Comput. Phys. 48 (3) (1982) 387–411, https://doi.org/10.1016/0021-9991(82)90058-4.
[65] M. Zhong, S. Zou, D. Pan, C. Zhuo, C. Zhong, A simplified discrete unified gas–kinetic scheme for compressible flow, Phys. Fluids 33 (3) (2021) 036103, https://doi.org/10.1063/5.0033911.